Correspondence to:
I. Grünberg,
inge.gruenberg@awi.de

Permafrost and Active Layer Temperature and Freeze/Thaw Timing Reflect Climatic Trends at Bayelva, Svalbard

Inge Grünberg[1], Brian Groenke[1,2], Sebastian Westermann[3], and Julia Boike[1,4]

[1]Permafrost Research Section, Alfred Wegener Institute Helmholtz Centre for Polar and Marine Research, Potsdam, Germany, [2]Department of Electrical Engineering and Computer Science, Technical University of Berlin, Berlin, Germany, [3]Department of Geosciences, University of Oslo, Oslo, Norway, [4]Department of Geography, Humboldt Universität zu Berlin, Berlin, Germany

Abstract Permafrost warming has been observed all around the Arctic, however, variations in temperature trends and their drivers remain poorly understood. We present a comprehensive analysis of climatic changes spanning 25 years (1998–2023) at Bayelva (78.92094°N, 11.83333°E) on Spitzbergen, Svalbard. The quality controlled hourly data set includes air temperature, radiation fluxes, snow depth, rainfall, active layer temperature and moisture, and, since 2009, permafrost temperature. Our Bayesian trend analysis reveals an annual air temperature increase of 0.9 ± 0.5°C/decade and strongest warming in September and October. We observed a significant shortening of the snow cover by −14 ± 8 days/decade, coupled with reduced winter snow depth. The active layer simultaneously warmed by 0.6 ± 0.7°C/decade at the top and 0.8 ± 0.5°C/decade at the bottom. While the soil surface got drier, in particular during summer, soil moisture below increased in accordance with the longer unfrozen period and higher winter temperatures. The thawed period prolonged by 10–15 days/decade at different depths. In contrast to earlier top-soil warming, we observed stable temperatures since 2010 and only little permafrost warming (0.14 ± 0.13°C/decade). This is likely due to recently stable winter air temperature and continuously decreasing winter snow depth. This recent development highlights a complex interplay among climate and soil variables. Our distinctive long-term data set underscores (a) the changes in seasonal warming patterns, (b) the influential role of snow cover decline, and (c) that air temperature alone is not a sufficient indicator of change in permafrost environments, thereby highlighting the importance of investigating a wider range of parameters, such as soil moisture and snow characteristics.

Plain Language Summary Permafrost is warming across the Arctic, but it is not yet well understood why temperature trends vary and what affects them the most. Our detailed study investigates 25 years (1998–2023) of data at the Bayelva permafrost observatory on Svalbard. We analyzed a quality-controlled data set, including hourly measurements of air temperature, radiation, snow depth, rainfall, permafrost temperature, and active layer conditions. We looked beyond annual averages, examining changes in each month. The air warmed strongly by 0.9°C/decade and even stronger in September and October. Continuous snow cover shortened by −14 days/decade and winter snow depth decreased. Simultaneously, the active layer warmed by 0.6°C/decade at the top and 0.8°C/decade at the bottom. While the surface dried in summer, deeper soil layers became moister due to a longer unfrozen period and higher temperatures in winter. The thawed period extended by 10–15 days/decade, with slightly stronger changes toward later freezing in autumn. We found that soil warming stopped in recent years and attributed this effect to the lower winter snow depth since 2010. Therefore, if we want to know how permafrost warms or cools in the future, we need to consider additional measurements such as soil moisture and snow properties.

1. Introduction

The drastic warming observed in the Arctic, which has exceeded the global average by nearly four times since 1979 (Rantanen et al., 2022), has profound implications for various cryospheric and meteorological variables, including rainfall, snow cover, and the thermal and hydrological characteristics of permafrost. Quantifying subsurface changes requires complex instrumentation or modeling and is addressed by a limited number of long-term data series. The impact of climatic changes and, in particular, of snow cover trends on permafrost is notably pronounced on the west coast of Svalbard.

Air temperature warming on Svalbard has been even stronger than the Arctic average with warming rates of about 1.5°C/decade (1991–2020) (Isaksen et al., 2022b; Nordli et al., 2020). This is linked with the strong sea-ice

decline in that region (Dahlke et al., 2020; Isaksen et al., 2016; Vihma, 2014). While warming was most pronounced during winter in the 1980s and 1990s, autumn warming has become more significant since then (Isaksen et al., 2022b). Higher temperatures and sea-ice decline led to increased precipitation in all seasons (Hanssen-Bauer et al., 2019; McCrystall et al., 2021) and a strong increase in the ratio of rainfall to snowfall (Bintanja & Andry, 2017; Hanssen-Bauer et al., 2019). The snow-covered period in Svalbard shortened by about 3.3 days/decade (1958–2017) with a stronger trend toward later last snow-free day in autumn as compared to earlier first snow-free day in spring (Hanssen-Bauer et al., 2019; van Pelt et al., 2019; Vickers et al., 2020). Due to the maritime climate, the west coast of Svalbard experiences rain-on-snow events even in mid winter (Wickström et al., 2020). Such events are getting more frequent due to autumn and winter warming (Bintanja & Andry, 2017; Hansen et al., 2014; Vickers et al., 2022). Strong rain-on-snow events are a significant source of energy for the snowpack and ultimately for the permafrost (Boike et al., 2003; Westermann et al., 2011). On the other hand, rain-on-snow also has the potential to destroy the snow structure and convert thermally insulating low density snow into more conductive high-density snow or even ice layers (Calonne et al., 2011). When cooling occurs after the rain-on-snow event, this snow metamorphism allows the soil to cool down more efficiently (Pomeroy & Brun, 2001). This may lead to a net soil cooling following rain-on-snow if it happens in early or mid-winter.

The observed drastic changes in climate variables affect the permafrost. Permafrost temperatures on Svalbard are often close to the freezing point, especially in the vicinity of the coasts in the south of the archipelago (Christiansen et al., 2020a; Hanssen-Bauer et al., 2019). Warming has been observed since instrumentation in 1998, as shown by long-term temperature data from the Janssonhaugen station in central Svalbard close to Longyearbyen (Isaksen et al., 2022a). This warming was especially pronounced at depths of 10 and 20 m. Additionally, near-surface permafrost had also warmed significantly (Boike et al., 2018), and the active layer depth at Janssonhaugen increased from 1.6 m (1999) to almost 2 m (2016) (Isaksen et al., 2022a). At a more coastal site in Adventdalen, the active layer depth increased by 0.7 cm/year (2000–2018) (Strand et al., 2021). These changes are indicative of a significant long-term shift in the permafrost thermal state, a commonly used indicator in international assessment reports. However, permafrost temperature alone does not fully define the thermal state in warmer permafrost regions where latent heat effects play a substantial role (Groenke et al., 2023; Smith et al., 2022). Depending on the soil properties, unfrozen water can remain present in the soil pores at temperatures well below 0°C (Nicolsky & Romanovsky, 2018). Therefore, additional measurements of volumetric liquid water content, referred to hereafter as soil moisture, are necessary to fully assess the thermal state of permafrost.

While the current state and recent trends in air and permafrost temperatures are relatively well established, there is a lack of long-term data on other meteorological drivers such as snow depth and liquid precipitation, hereafter referred to as rainfall. Furthermore, there is a lack of data describing the thermal state of the active layer including soil moisture. Due to this knowledge gap, relying only on air temperature trends is insufficient to draw conclusions about permafrost vulnerability in regions with warmer permafrost such as Svalbard.

Our study contributes to filling this gap by quantifying current climatology and trends (1998–2023) for both climatic drivers as well as thermal and hydrological conditions in permafrost affected soil (hereafter referred to simply as "soil") at the Bayelva study site close to Ny-Ålesund, Svalbard. We quantify trends in temperature, radiation fluxes, rainfall, and snow cover. We then compare them to trends in active layer moisture and temperature and analyze the seasonality of the observed changes. Furthermore, we relate the most important climatic drivers to permafrost temperatures for the years 2010–2023.

2. Soil and Climate Data

2.1. Field Site

The Bayelva permafrost and climate observatory is located near Ny-Ålesund, Svalbard (78.92094°N, 11.83333°E, Figure 1). It is a High Arctic site located on the Leirhaugen hill (25 m a.s.l.) currently 2 km north of the rapidly retreating tongue of the Brøggerbreen glacier. The Leirhaugen hill is covered with permafrost patterned ground and sparse vegetation (prostrate dwarf-shrub, herb tundra, P1 in the classification by Walker et al. (2005)). The soil contains large stones and gravel within silty material (Boike et al., 2018). The permafrost depth nearby the site, at the foot of the Zeppelinfjellet, is around 130–140 m (Orvin, 1944). Detailed descriptions of the site including climatology and active layer properties are provided in Boike et al. (2008, 2018), and Westermann et al. (2009).
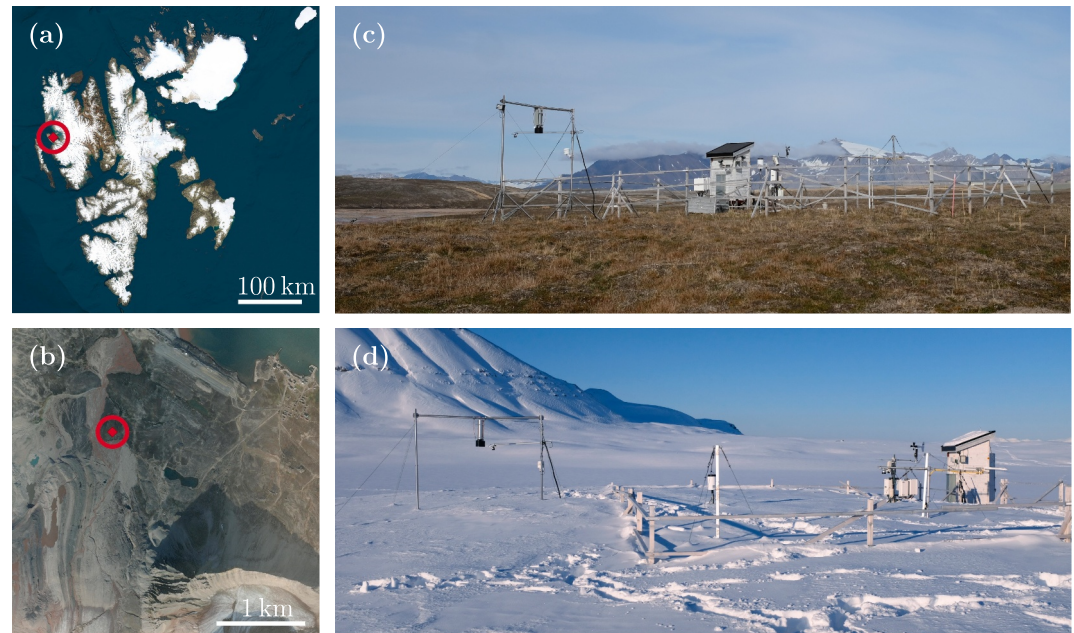
Figure 1. Location of the Bayelva permafrost and climate observatory on Svalbard (a) and in the Bayelva river basin near Ny-Ålesund (b) and pictures of the site in summer 2023 (c) and in winter 2021 (d); basemap source: Esri Satellite (Esri, DigitalGlobe, GeoEye, i-cubed, USDA FSA, USGS, AEX, Getmapping, Aerogrid, IGN, IGP, swisstopo, and the GIS User Community).

2.2. Data Sources

The Bayelva permafrost and climate observatory features a unique 25 years data series (13 September 1998 to 2 January 2024) of the main meteorological variables including soil temperature and moisture in different depths representing the complete active layer. The data set used in our study is merged from two soil profiles in the same fenced measurement area with the first profile operating 1998–2009 and the second 2009–today. The measurement depths of 3, 10, 22, 38, 58, 73, 94, and 135 cm were chosen to represent all major soil horizons and had to be adjusted to avoid the frequent rocks within the soil. While the soil sensors cannot be exchanged, the climate sensors were regularly exchanged and calibrated. The soil and climate measurement setup, choice of sensors and calibration routines are described in detail in Boike et al. (2018). The climate data includes air temperature measured with PT-100 and Vaisala HMP45 (since 2009), snow depth measured with Campbell Scientific SR50 ultrasound sensors and a Jenoptik SHM30 laser distance sensor (since 2013), rainfall measured with a Young 52203 unheated tipping bucket rain gauge, and radiation components measured with Campbell Scientific Q7, Kipp & Zonen NR Lite, Skye Pyranometer SP1110, and Hukseflux NR01 (since 2009). The soil moisture profile down to 1 m depth is measured with Time Domain Reflectometry probes (TDR Tektronix 1502B with TDR triple-wire 0.24 m long probes until 2009 and TDR100 with 0.3 m long triple-wire Campbell Scientific CS605 probes since 2009). The soil temperature profile down to 1.4 m is instrumented with Campbell Scientific 107 thermistors.

Additionally, permafrost temperatures at up to 9 m depth are measured since 18 August 2009 (Geoprecision temperature chains with 10 sensors: M-Log 2009–2023 and TNode HD since 2021). Detailed descriptions of the laboratory and field calibrations, instrumentation, data preprocessing, and flagging routines are provided in Boike et al. (2018). For validation and intercomparison, we used data from The Norwegian Meteorological Institute (MET Norway) (2024) (https://seklima.met.no/observations) collected in Ny-Ålesund, roughly 2 km to the north-east, at the shore of Kongsfjorden. The Ny-Ålesund data includes mean daily values of air temperature, precipitation, snow depth, and spatial snow cover fraction. The latter is estimated by an observer in a radius of 1 km around the station.

2.3. Data Quality Control and Preprocessing

The quality control routine of the Bayelva meteorological data is described in detail by Boike et al. (2018). For soil temperature and soil moisture, we used the level 2 data set which is combined from two different soil profiles

for the periods 1998–2009 and 2009–today (Boike et al., 2018). We did not modify the hourly data in any way (e.g., no interpolation or regression). However, we replaced all flagged data points with NaN. We used air temperature at 1 m height to gapfill the 2 m air temperature. Both sensors measured simultaneously and reliably except for the period 3 September 2008 to 22 October 2008 when the data at 2 m height was missing. Given the lack of tall vegetation, the difference between the two heights is marginal ($R = 0.9963$, regression slope $= 1.0176$). Snow depth is a combination of four sensors which are described in Boike et al. (2018). All data was processed in UTC (e.g., for daily averages). We published the quality-controlled dataset in Grünberg et al. (2024a).

The analysis of the climatology and the trends required data aggregation to daily, monthly, seasonal, and annual values. The recent climate data has half-hourly resolution. We resampled this data to hourly data by taking the mean of the two values. In case one was missing, we used the remaining value as hourly measurement. During the resampling of hourly data to longer periods, we applied linear interpolation of short gaps and thresholds of how many persisting gaps were allowed for a mean value to be computed. We interpolated gaps of up to 6 hr linearly in the hourly time series before aggregating it to a daily series. Days containing longer gaps or less than 12 hourly data points were treated as missing data. Gaps up to 3 days were interpolated linearly in the daily time series before aggregating it to a monthly series. Months containing longer gaps were treated as data gaps. Gaps up to 1 month were interpolated linearly in the monthly time series before aggregating it to an annual series. Years containing longer gaps were treated as missing data. For seasonal trends, we used the months January to March as winter. While this may be inconsistent with the standard definition (December–February), it is a more suitable definition for Arctic regions where March is often the coldest month of the year. March is also the month with least liquid precipitation. Due to the cold March air temperature, the insulating effects of snow, an important winter feature, are most critical. We defined summer in accordance with the general definition as June to August, which are also the months with highest average air temperature.

To summarize the climatology at the Bayelva permafrost and climate observatory, we resampled the half-hourly and hourly data to daily data. We used the daily sum for rainfall and the mean for all other variables. We computed the median, 5th and 95th percentile of all daily values within calendar weeks. For example, we used all mean daily air temperature values of days of the year 1–7 of all years for the median of week 1. In the case of rainfall, we additionally computed the mean because the median is zero for most weeks of the year.

2.4. New Data Sets of Spatial Snow Cover and Soil Freeze/Thaw State

We estimated the spatial cover fraction of snow at daily resolution at Bayelva using webcam images (2007–2023). For earlier years and gapfilling, we established a relationship between this reference snow cover and the snow depth measured at a single location in Bayelva. The complete routine is described in Appendix A.

We derived the freeze/thaw state of the active layer based on the soil temperature at approx. 3, 10, 22, 38, 58, 73, 94, and 135 cm depth. We divided the data at each depth based on its temperature into three categories: (a) warm ($T > 0.2°C$), (b) zero curtain ($-0.5°C < T \leq 0.2°C$), and (c) cold ($T \leq -0.5°C$) (Figure 2). The thresholds of -0.5 and $0.2°C$ were set pragmatically rather than based on physical properties of freezing, as water under standard conditions freezes at 0°C. These thresholds account for the measurement uncertainty noted in sensor data, which generally tend to underestimate temperatures. We derived these values from analyzing the zero curtain periods and the temperature distributions of each sensor. Based on the time series of temperature conditions (Figure 3a), we estimated the start of thawing in spring and the start of freezing in autumn (see Appendix B for details).

2.5. Trend Analysis

Our trend analysis of all variables was based on monthly and annual mean (sum for rainfall) values. For monthly values, we created 12 time series of each variable containing all years of one specific month (e.g., January). We analyzed long-term trends for the time-averaged variables Y_i sampled at times $t = 0, 1, \ldots, n$ years since the beginning of the study period using a Bayesian generalized linear model (GLM):
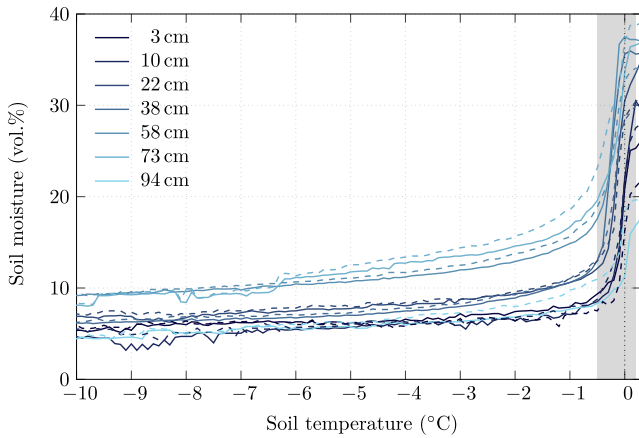
Figure 2. Median of all annual freeze curves at each soil depth calculated from data of each freezing/thawing season (1998–2023) separately; annual freeze curves were derived from median soil moisture values within 0.1°C soil temperature bins; solid lines: thawing, dashed lines: freezing; the gray shaded area is the temperature range defined as zero curtain.

$$\tilde{y}_i \sim \text{GLM}(\eta_i, \xi_i, f_i)$$
$$\eta_i = \mu_i + \beta_i t$$
$$\beta_i \sim \mathcal{N}(\mu = 0, \sigma = \sigma_\beta(Y_i))$$
$$\mu_i \sim \mathcal{N}(\mu = \mu(Y_i), \sigma = \sigma_\mu(Y_i))$$
$$\xi_i \sim \pi_i(\phi)$$

where β_i and μ_i are the slope and intercept for the linear response η_i, t is the time offset in years, f_i is an appropriate link function for variable i, and ϕ are hyperparameters for the GLM auxiliary parameter prior π_i. For variables with an effectively unbounded domain on the real line (e.g., temperature and net radiation), we chose the Student-t distribution as the GLM likelihood with $f_i(y) = y$ due to the relatively small number of observations (fewer than 25 years for all variables) and the possibility of non-normal interannual variation. The Student-t likelihood is generally considered to provide more conservative estimates of effect sizes that are less sensitive to outliers and heteroscedasticity which are common in small data sets (Gelman et al., 2013; Lange et al., 1989). For variables with a semipositive domain $[0, \infty)$ (e.g., rainfall and snow depth), we selected the Gamma distribution as the likelihood with $f_i(y) = \log(y)$ to model all nonzero observations. Finally, for variables with double bounded domains in the unit interval $[0, 1]$ (e.g., soil moisture) we chose the Beta distribution as the likelihood with $f_i(y) = \text{logit}(y)$. We used the python packages `bambi` (BAyesian Model Building Interface) (Capretto et al., 2022) and `pymc` (Wiecki et al., 2023) to construct and fit all of the trend models. The hyperparameters for the priors of β_i and μ_i were determined automatically from the data Y_i by the `bambi` software using the methodology described in Capretto et al. (2022). We simulated a total of 14,000 samples from four parallel Markov Chains using the No-U-Turn sampling method of Hoffman and Gelman (2014) with the first 2,500 samples from each chain discarded as warm-up.

2.6. Reporting of Trend Estimates

Boxplots present the interquartile range of the posterior trend estimates within the box, the median as the middle line, and the 5th and 95th percentiles as whiskers. In some figures, the uncertainty is given as a shaded area representing
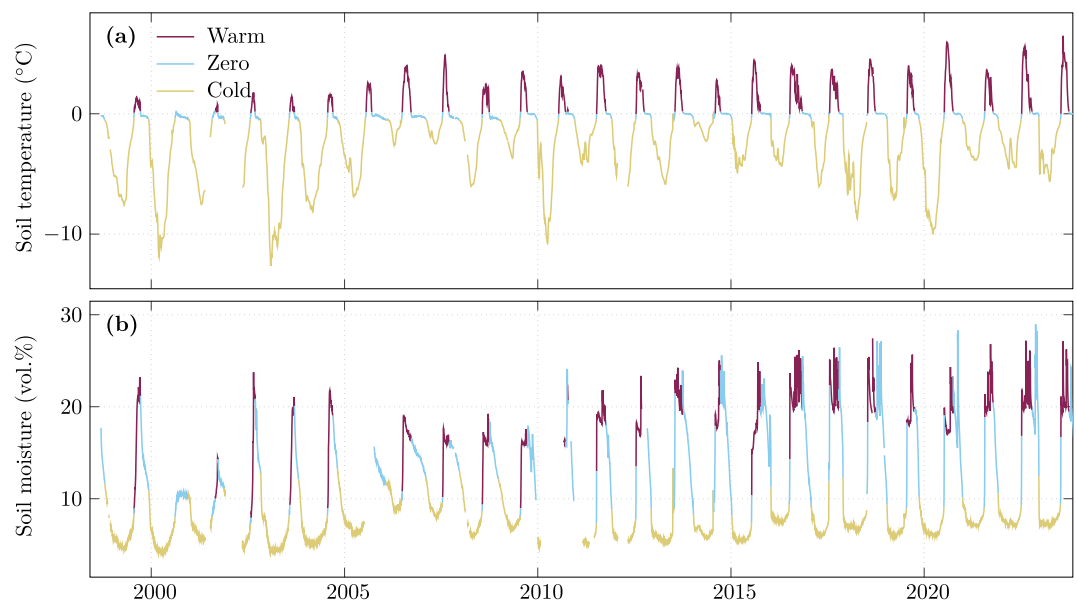

Figure 3. Time series of daily active layer temperature (a) and moisture (b) at 94 cm depth. The colors indicate the temperature state of the soil with warm ($T > 0.2$°C), zero curtain (-0.5°C $< T \leq 0.2$°C), and cold ($T \leq -0.5$°C) conditions.

the 5th to 95th percentiles of the estimations. Numbers of estimated trends represent the median value plus/minus the uncertainty range representing the mean of the difference of 5th and 95th percentile to the median estimate. The percentage of posterior trend estimates smaller/greater than zero (depending on the sign of the median) is provided in brackets. For example, a trend of 0.091 ± 0.049°C/year (100%) means that the estimated trend is 0.091°C/year. This is the median of all samples. The symmetrized 90% confidence interval covers 0.049°C/year in each direction. In this particular example, the fifth percentile of possible trends given the data is 0.044°C/year and the 95th percentile 0.143°C/year. The posterior probability that the trend shows an increase is 100%. Variables with least 90% positive trend estimates are described as "increasing", with no more than 10% positive trends as "decreasing". Other trends are described as more uncertain. To provide a visual impression of the confidence, the values presented in result tables are colored. Trends with at least 90% of the trend estimates pointing in the same direction as the median are presented in black, 80%–90% in dark gray, and less than 80% in light gray. These light gray values should not be over-interpreted. In the results and discussion sections, all trends are provided in `measurement unit per year`. For consistency, we also converted the trends which were reported `per decade` in literature to `per year`.

3. Results

3.1. Air Temperature, Rainfall, and Snow

We analyzed the climatology and trends for air temperature, rainfall, and snow depth and coverage because these are the major drivers of changes in the soil thermal regime. In the period 1998–2023, the average air temperature varied between −15°C (February/March) and 7°C (July) with much larger variability in winter as compared to summer (Figure 4a). The coldest month of the record was December 2003 with −19.8°C and the warmest month was July 2020 with 9.2°C on average. We observed rapid air temperature warming at Bayelva. Between 1999 and 2023, mean annual air temperature increased by 0.091 ± 0.049°C/year (100%) (Figure 4b and Table 1). The strong warming trend was observed in each month of the year with the strongest warming in September and October (Figure 4c and Table 1). Due to the high interannual variability, winter trends showed a higher uncertainty. Between 1999 and 2023, net radiation increased by 0.26 ± 0.26 W/m^2/year (94%) while incoming shortwave radiation increased by 0.29 ± 0.21 W/m^2/year (99%) (Table 1).

We observed high interannual variability in winter snow depth with the onset of melt falling between beginning of June and the first week of July (Figure 4d). Mean monthly snow depth decreased in the autumn and winter months with the strongest decrease of almost 1 cm/year in October (Figure 4f and Table 1). On the other hand, April and May snow depth remained approximately stable and the maximum annual snow depth did not change over time (Table C1). However, the observed snow depth trends had a high uncertainty due to the interannual variability. Trends in timing of the snow cover build-up and melt as well as the duration of a spatially closed snow cover were much stronger and had a higher confidence (Figure 4e and Table C1). While the spatially closed snow cover duration decreased by −1.4 ± 0.8 days/year (100%), the number of completely snow-free days increased by 0.9 ± 0.5 days/year (100%). The difference between the two values was caused by an increase of partially snow-covered conditions. Furthermore, we observed a tendency toward an earlier onset of the melting period as defined by the first snow-free patches at Bayelva by −0.43 ± 0.61 days/year (88%).

At Bayelva, rainfall occurred throughout the year (Figure 4g). While the median daily rainfall was 0 mm in most weeks of the year, the highest values were reached in late August and September. Total annual rainfall showed a rising trend of 4.90 ± 7.38 mm/year/year (87%). However, the interannual variability of annual rainfall was large, which led to a considerable uncertainty of the trend estimate (Figure 4h). This interannual variability also affected the trends of total monthly rainfall. The winter period of December to beginning of April rarely had rainfall events, but we observed single strong rainstorms. These rain-on-snow events were too rare to be analyzed statistically for a period of 25 years, at least on a monthly basis (missing data in Figure 4i). We observed the strongest trends of increasing rainfall in May, June, and November and somewhat less certain increases in April and September (Table 1). The total winter (January–March) rainfall trends were highly uncertain but pointed toward an increase. On the other hand, rainfall trends in July and October tended to be negative between 1998 and 2023 (Figure 4i).

3.2. Active Layer Temperature and Moisture

As expected, intraannual variability of active layer temperature decreased with depth (Figure 5a). Lower depths showed a delayed response to climate forcing and generally less interannual variability. The upper part of the active layer warmed more slowly than air temperature (0.06 ± 0.07°C/year [91%]), while lower depths (at 94 and

Figure 4. (a, d, g) Median and variability (5th to 95th percentile) calculated from all daily data for every 7 days of the period 1998–2023 for climate variables; (b, e, h) annual values and the respective trend; (c, f, i) trends of mean monthly values for (a)–(c) air temperature, (d)–(f) snow depth and duration of a spatially continuous snow cover, (g)–(i) rainfall (the mean is included as dotted line).

135 cm) warmed with a similar rate as air temperature (Figure 5b and Table C2). We observed clear evidence of warming across all depths and months except during freeze curtain conditions from October to December (Figure 5c). The sensors at most depths showed the strongest warming in April and August. Winter trends showed the largest uncertainties at all depths.

Soil moisture within the active layer experienced a strong increase in June or beginning of July, corresponding to snow melting and soil thawing (Figure 5d). Different soil depths showed different summer soil moisture levels depending on their porosity and saturation conditions. While soil moisture of the top layer decreased between 1999 and 2023, all other depths revealed an increase in moisture (Figure 5e and Table C3). The smallest increase was observed at 38 cm depth, in a layer of carbon rich soil due to the naturally occurring coal (Table F1 in Boike et al. (2018)). This layer has a different texture than the surrounding soil (Boike et al., 2018). Unlike for soil temperature, the soil moisture trends revealed clear differences between the seasons. At 3 cm, the soil moisture decreased in all months with a particularly strong decrease in July and August (Figure 5f). This summer decrease could also be observed at 10 cm depth, whereas soil moisture increased in the other months at this depth (Table C3). At all lower depths, soil moisture increased all year around. While the soil moisture increase was small during frozen conditions, summer and autumn showed the strongest wetting trends.

Table 1
Trend Estimates for Main Climate Variables Between October 1998 and December 2023 (Top) and Between January 2010 and December 2023 (Bottom); Winter Is Defined as January–March Representing the Three Coldest Months, Summer Is June–August

	Air temperature °C/year	Rain mm/interval/year	Snow depth cm/year	Net radiation W/m²/year	Shortwave incoming W/m²/year
October 1998 to December 2023					
Annual	0.091 ± 0.049 (99.9%)	4.9 ± 7.4 (87.0%)	−0.35 ± 0.67 (82.9%)	0.26 ± 0.26 (94.0%)	0.29 ± 0.21 (98.6%)
Summer	0.097 ± 0.033 (100.0%)	0.5 ± 2.1 (66.4%)		1.12 ± 0.59 (99.8%)	0.74 ± 0.79 (93.7%)
Winter	0.100 ± 0.110 (93.6%)	1.2 ± 6.8 (67.9%)	−0.47 ± 1.28 (74.0%)	−0.36 ± 0.22 (99.8%)	
January	0.122 ± 0.195 (85.6%)		−0.63 ± 1.46 (78.3%)	−0.57 ± 0.31 (99.8%)	
February	0.097 ± 0.166 (83.4%)		−0.44 ± 1.46 (70.7%)	−0.09 ± 0.34 (66.9%)	
March	0.082 ± 0.170 (79.1%)		−0.50 ± 1.26 (75.9%)	−0.48 ± 0.33 (98.8%)	0.12 ± 0.12 (94.9%)
April	0.132 ± 0.151 (92.5%)	0.3 ± 0.7 (84.5%)	−0.17 ± 1.08 (60.8%)	0.24 ± 0.41 (83.2%)	0.64 ± 0.68 (93.7%)
May	0.046 ± 0.077 (84.5%)	1.2 ± 1.0 (99.5%)	−0.14 ± 1.33 (57.9%)	0.72 ± 0.47 (99.2%)	0.53 ± 0.94 (82.4%)
June	0.092 ± 0.042 (99.9%)	0.5 ± 0.7 (91.3%)	−0.46 ± 1.80 (69.9%)	2.13 ± 1.21 (99.7%)	−0.12 ± 1.35 (55.8%)
July	0.115 ± 0.044 (100.0%)	−0.4 ± 1.4 (73.0%)		0.80 ± 0.77 (94.9%)	1.22 ± 0.95 (98.0%)
August	0.082 ± 0.041 (99.9%)	0.3 ± 1.1 (71.5%)		0.54 ± 0.42 (97.9%)	0.96 ± 0.52 (99.8%)
September	0.134 ± 0.087 (99.2%)	1.1 ± 2.2 (81.6%)	−0.30 ± 0.43 (97.9%)	0.45 ± 0.43 (95.7%)	0.09 ± 0.20 (78.3%)
October	0.139 ± 0.107 (98.2%)	−1.2 ± 2.7 (84.2%)	−0.92 ± 0.89 (98.7%)	−0.25 ± 0.26 (94.2%)	−0.00 ± 0.02 (55.5%)
November	0.072 ± 0.149 (79.3%)	1.8 2.7 (93.0%)	−0.57 ± 1.09 (83.0%)	−0.41 ± 0.32 (98.2%)	
December	0.091 ± 0.107 (92.7%)		−0.63 ± 1.19 (82.2%)	−0.43 ± 0.36 (97.7%)	
January 2010 to December 2023					
Annual	0.080 ± 0.114 (88.1%)	−5.93 ± 21.31 (71.0%)	−0.68 ± 1.44 (80.6%)	−0.47 ± 0.50 (94.5%)	−0.30 ± 0.50 (84.9%)
Summer	0.122 ± 0.093 (98.0%)	1.72 ± 7.21 (67.3%)		−0.79 ± 1.11 (87.6%)	−0.97 ± 1.59 (84.7%)
Winter	0.093 ± 0.329 (68.4%)	−6.53 ± 18.31 (86.5%)	−1.25 ± 2.63 (79.7%)	−0.17 ± 0.39 (76.5%)	
January	−0.059 ± 0.448 (58.6%)		−1.80 ± 3.21 (85.6%)	−0.96 ± 0.55 (99.7%)	
February	0.075 ± 0.499 (60.2%)		−2.14 ± 2.98 (90.6%)	0.76 ± 0.81 (93.7%)	
March	0.080 ± 0.396 (63.6%)		−0.38 ± 2.28 (61.9%)	−0.37 ± 0.73 (80.6%)	−0.14 ± 0.46 (69.4%)
April	0.079 ± 0.298 (67.7%)	0.95 ± 2.71 (84.2%)	−0.38 ± 2.80 (59.9%)	−1.21 ± 0.84 (98.2%)	−1.00 ± 1.75 (83.2%)
May	−0.061 ± 0.201 (69.8%)	1.94 ± 2.27 (96.4%)	0.18 ± 3.43 (53.7%)	−1.33 ± 0.75 (99.7%)	−0.33 ± 2.52 (59.2%)
June	0.051 ± 0.105 (79.7%)	0.02 ± 1.95 (50.7%)	−0.47 ± 4.50 (59.4%)	−1.01 ± 2.85 (72.1%)	−3.10 ± 2.83 (96.1%)
July	0.182 ± 0.123 (98.9%)	−0.11 ± 3.80 (52.2%)		−0.41 ± 1.33 (70.4%)	0.83 ± 2.68 (70.3%)
August	0.115 ± 0.112 (95.2%)	1.59 ± 3.60 (81.4%)		−0.77 ± 0.55 (98.4%)	−0.84 ± 1.25 (87.1%)
September	−0.006 ± 0.212 (52.0%)	0.96 ± 6.59 (61.2%)	0.12 ± 0.51 (74.3%)	−1.12 ± 0.80 (98.5%)	0.06 ± 0.53 (58.5%)
October	0.026 ± 0.250 (57.5%)	−5.71 ± 7.72 (97.7%)	−1.02 ± 1.63 (91.5%)	−0.33 ± 0.78 (77.6%)	0.01 ± 0.04 (61.2%)
November	0.306 ± 0.382 (91.1%)	−0.32 ± 8.52 (54.0%)	−1.05 ± 2.20 (82.1%)	0.29 ± 0.79 (73.7%)	
December	0.167 ± 0.186 (93.0%)		−1.63 ± 2.53 (88.3%)	−0.36 ± 1.05 (72.7%)	

Note. Trend estimates provided as median of all samples ± symmetrized 90% confidence interval (posterior probability that the trend direction is the same as the direction of the median); trend estimates with high confidence are shown in black, medium confidence in dark gray, and low confidence in light gray.

3.3. Freeze/Thaw State

As indicated by active layer temperature and moisture trends, the freeze/thaw timing of the active layer changed between 1998 and 2023. The sensor at 94 cm depth was at the lower boundary of the active layer in 1998 (Figure 3a), while the sensor at 135 cm depth remained permanently frozen until August 2004. The observed changes in the freeze/thaw state were most pronounced at these depths (Figure 6). At 73 cm and above, the number of warm and thawed days increased by 1.0 to 1.5 days/year (Figure 6a and Table C4). This agrees with the trend estimates of the lengthening of the snow-free period (Table C1). The shift toward later freezing in autumn

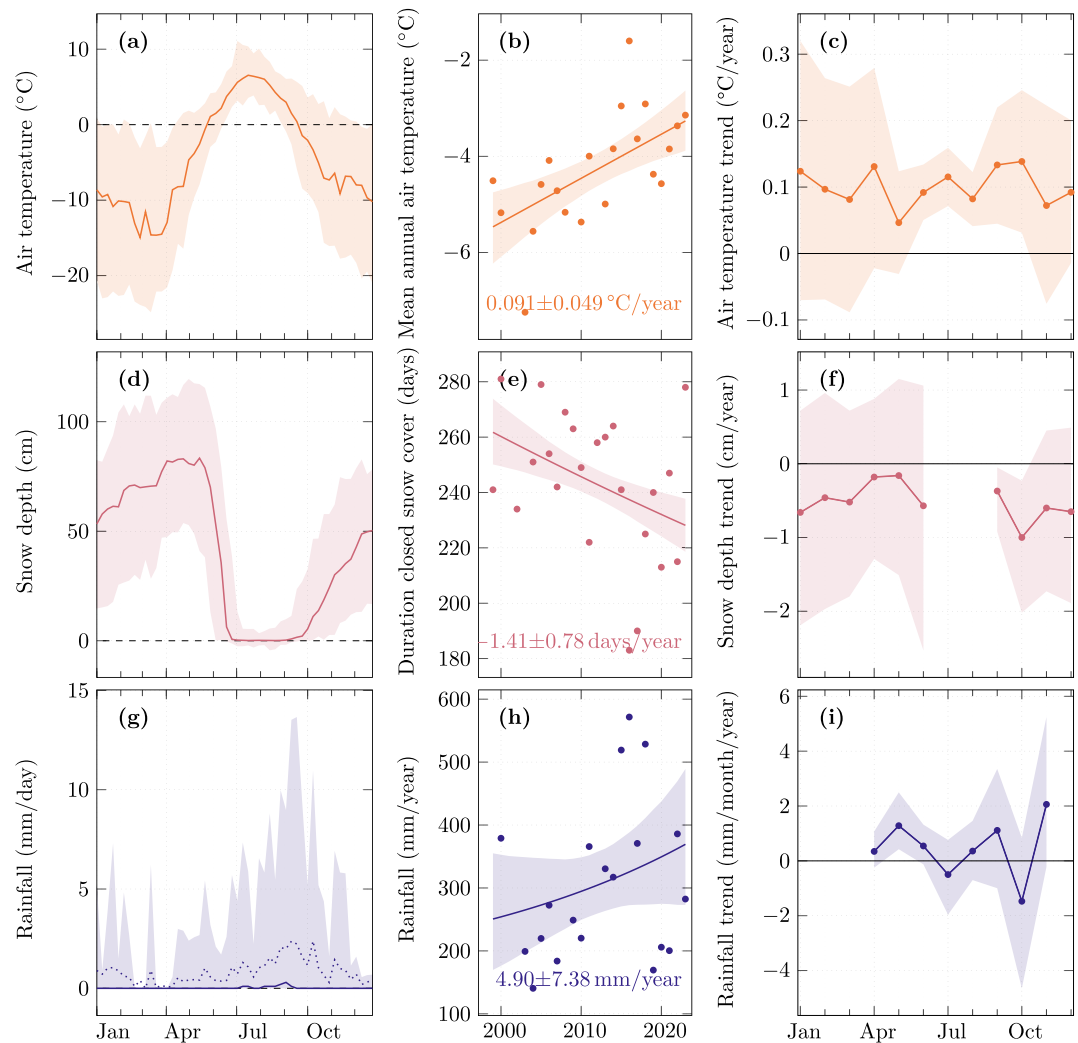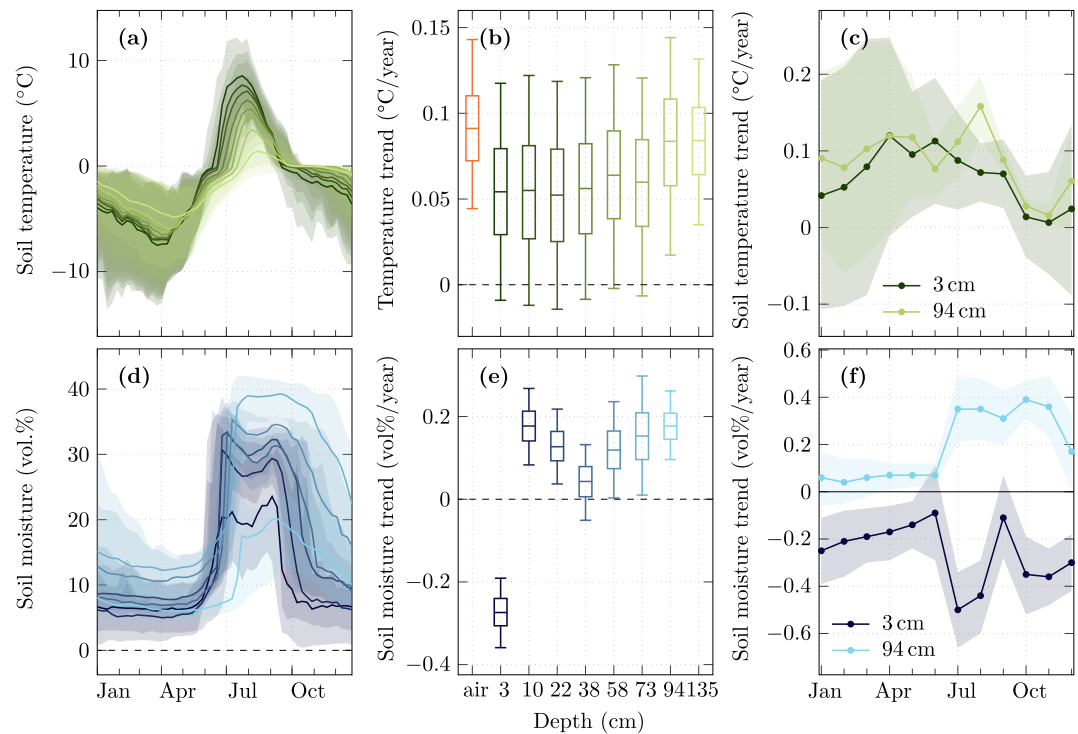**Figure 5.** (a, d) Median and variability (5th to 95th percentile) calculated from all daily data for every 7 days of the period 1998–2023 for active layer conditions; (b, e) trends of mean annual values in air and 8 (7) depths for active layer temperature (moisture); (c, f) trends of mean monthly values for (a)–(c) active layer temperature at different depths, see x-axis of panel (b/e) as legend, (d)–(f) soil moisture in the active layer at different depths, see x-axis of panel (e) as legend.

was slightly more pronounced than earlier thawing in spring, except for the surface at 10 cm and above (Figures 6b and 6c).

3.4. Permafrost Temperature and Trends Since 2010

Permafrost at the Bayelva permafrost and climate observatory warmed by 0.014 ± 0.013°C/year (95%) at 9 m depth (2010–2023, Figure 7a and Table C5). As compared to air and active layer warming between 1999 and 2023 (Figure 5b), this warming rate was relatively low. A closer look at permafrost temperatures revealed considerable interannual variation. Rising permafrost temperatures between 2011 and 2017 were followed by slightly lower temperatures in 2018 and 2019 and a strong drop in 2020 (Figure 7a). The cool permafrost temperatures in 2011 as compared to 2010 were likely a delayed response to the very cold active layer temperatures in January–March 2010 (Figure 3a). A possible reason was the heavy rain-on-snow event 15–25 January 2010 which may have destroyed the snow structure and made the snow cover more thermally conductive. In that winter, soil temperature followed the cold air temperature much more closely than in other winters (Figure 3a). The sharp drop in permafrost temperatures in 2020 coincides with a combination of very cold winter air temperature and low snow depth in early 2020 (Figure 8). While the warmest two winters were associated with warming permafrost (blue circles in Figure 8), the two winters with the thinnest snow cover (less than 40 cm) were associated with cooling permafrost (red circles in Figure 8). Summer air temperature, on the other hand, may have been an influential factor in the years 2022 and 2023 (Figure 8d). As summer is in the middle of the year, the impact of summer air temperatures on permafrost temperatures may also be delayed until the following year.

Our data series for permafrost temperature started in summer 2009. We therefore repeated the trend analysis of all climate and active layer variables for this period. We found that the annual air temperature trend was a bit lower for 2010–2023 as compared to 1999–2023 (Table 1). As expected for the shorter period, the uncertainty was much higher than for the longer period. The continued warming of the annual mean air temperature was caused by strong warming in summer (June–August), November, and December (2010–2023, Table 1). July, August, November, and December were also the only months which had stronger trends for 2010–2023 than 1998–2023
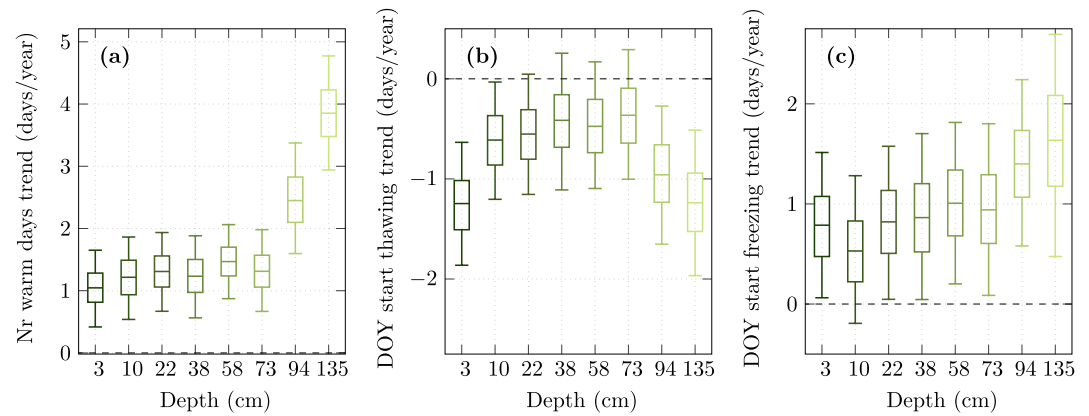
Figure 6. (a) Trend in number of days with above 0°C temperature, (b) shift in the onset of spring thawing which is the first Day Of Year (DOY) when 0°C is reached, and (c) shift in the onset of autumn freezing which is the last day when the temperature is above 0°C before the soil is frozen for at least 10 consecutive days.

(Figure 7c). Trends for January to May were very uncertain and air temperature cooling was possible, in particular in May (Figure 7c and Table 1). The strong autumn warming described above for 1998–2023 was restricted to November while air temperature of September and October did not rise anymore between 2010 and 2023. The lack of a winter warming trend co-occurred with a strong decrease of winter snow depth by −1.6 to −2.1 cm/year in the months December, January, and February since 2010 (Figure 7d and Table 1). In these early winter months, the decreasing trend strongly intensified as compared to the complete period 1999–2023. However, given the short period and the high inter-annual variability all estimated snow depth trends were more uncertain than for the
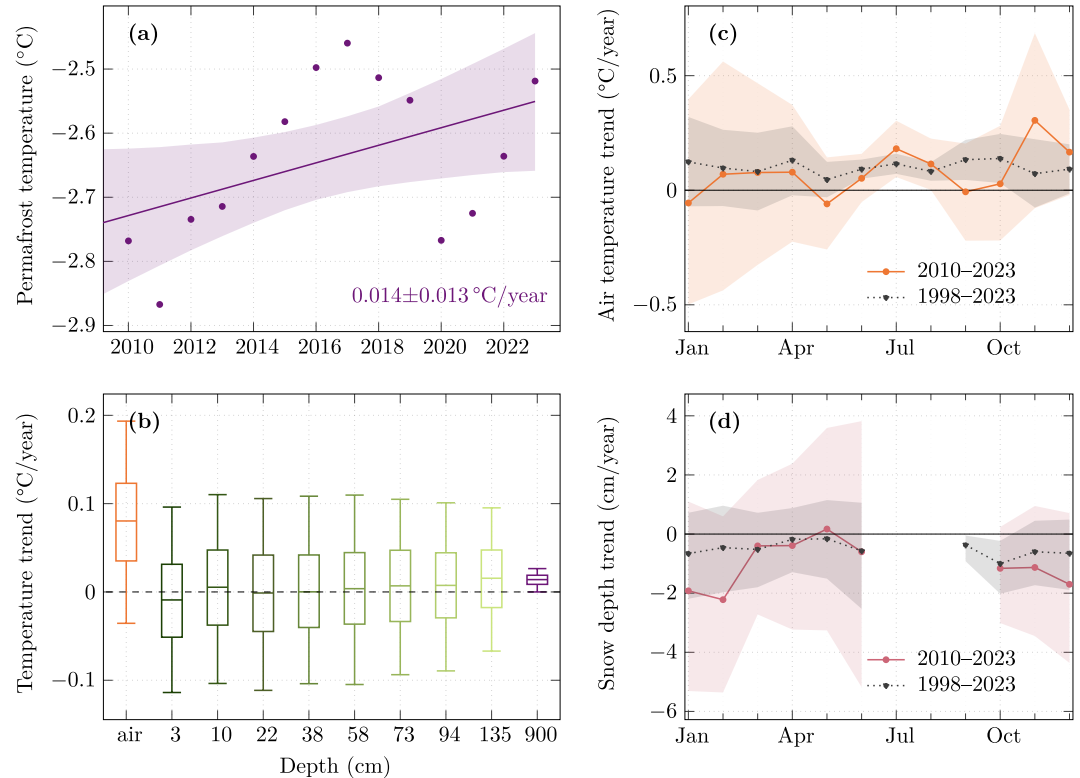
Figure 7. Trend estimate for the shorter period of 2010–2023; (a) Mean annual permafrost temperature at 9 m and the respective trend; (b) trends of mean annual values in air temperature, active layer temperature at 8 depths, and permafrost temperature at 9 m depth; (c) monthly air temperature trends (orange: 2010–2023, gray: 1998–2023) and (d) monthly snow depth trends (purple: 2010–2023, gray: 1998–2023).

Figure 8. (a) Mean annual permafrost temperature at 9 m; (b) mean winter (January–March) snow depth, (c) mean winter (January–March) air temperature, and (d) mean summer (June–August) air temperature; the 2 years with the warmest winter air temperatures are highlighted in blue and the 2 years with the thinnest snow cover in winter are highlighted in red; the effect of thin snow and warm winters on permafrost temperature is highlighted with arrows.

complete period. Annual average snow depth showed an uncertain but likely decreasing trend (Figure D1). Furthermore, the period 2010–2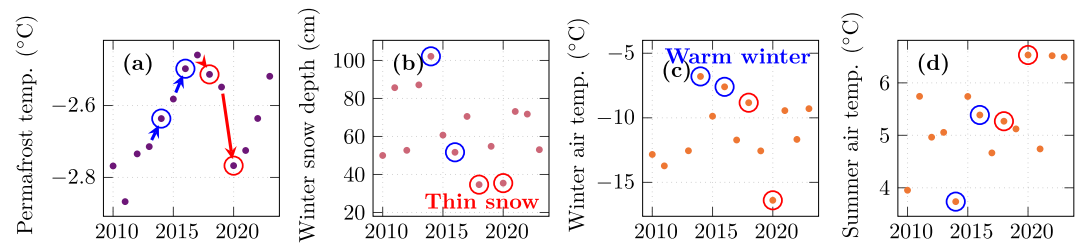023 was characterized by a decrease of annual average net radiation and, less certain, incoming shortwave radiation (Table 1).

Soil temperature trends within the shorter period were more uncertain than in the longer period. Furthermore, they showed no trend within the active layer and only a small positive trend of 0.014 ± 0.013°C/year (95%) in the permafrost at 9 m depth (Figure 7b). Related to the stop of an active layer warming trend (Table C2), we observed a trend toward drying of the active layer at 73 cm and above for 2010–2023 (Table C3).

4. Discussion

4.1. Air Temperature, Rain, and Snow

4.1.1. Air Temperature

We observed remarkable changes in all climatic variables between 1998 and 2023. Air temperature warming has been observed at many Arctic sites, with Svalbard showing generally higher rates than the Arctic average (Isaksen et al., 2022b). However, other sites in the High Arctic showed similar rates, such as Station Nord in Greenland with 0.08°C/year, 1990–2020 (Strand et al., 2022). For Svalbard specifically, Isaksen et al. (2022b) found that with 0.11°C/year Ny-Ålesund (2 km from Bayelva) had the weakest warming rate in two periods, 1991–2020 and 2001–2020, while eastern Svalbard in particular was warming more rapidly at more than 0.2°C/year. Using the same period and method, we found that air temperature trends at Ny-Ålesund and Bayelva agreed well for 1999–2023 (0.09 ± 0.05°C/year [100%]), although in absolute terms, Bayelva was about 1°C colder (brief results and Figure D1a in the Appendix). The lower trend in our data as compared to literature was due to the specific periods chosen. At the Bayelva permafrost and climate observatory, the last 4 years (2019–2023) were colder than 2015, 2016, and 2018. Furthermore, our data set started after the years 1993–1998, which were fairly cold in Ny-Ålesund (The Norwegian Meteorological Institute (MET Norway), 2024). Warming accelerated since the 1990s, as the air temperature trend 1950–2021 near Ny-Ålesund was lower with 0.06°C/year (Aga et al. (2023), based on downscaled ERA-5 reanalysis data).

We observed the strongest air temperature warming in autumn (Figure 4c). This agrees well with circum-Arctic patterns of the Arctic amplification (Rantanen et al., 2022). It is also in line with observations by Isaksen et al. (2022b) for western Svalbard, and Ny-Ålesund in particular, during the period 2001–2020. However, if the 1980s or 1990s are included, winter warming is even more pronounced than autumn warming (Gjelten et al., 2016; Isaksen et al., 2022b). This may be due to the massive change in sea-ice cover during that period (Isaksen et al., 2016). For the most recent period (2010–2023), we observed a lack of warming in some autumn and winter months (September, October, January) combined with amplified warming in July, August, and November (Figure 7c). To our knowledge, this recent shift toward summer driven warming has not yet been described in literature.

4.1.2. Rainfall

Trends in rainfall and snowfall have received much less attention than air temperature warming. Several studies report increasing precipitation in the Arctic (McCrystall et al., 2021; Vihma et al., 2016). In general, rainfall is

expected to increase more strongly than total precipitation because of an increase in the rain/snow ratio (Bintanja & Andry, 2017; Hanssen-Bauer et al., 2019). We observed a rainfall increase of 4.9 ± 7.4 mm/year (87%) in 2000–2023.

We measured a mean total rainfall (2000–2023) of 84 mm for the summer season, June–July–August. Despite the high interannual variability (24 mm in 2010 to 234 mm in 2013), the mean summer value matches the mean value of 84 mm measured in Ny-Ålesund in the years 1979–2018 by Førland et al. (2020). They report an uncorrected total annual precipitation of 447 mm for the same site and period. While total precipitation increased by 13%/decade, the solid fraction of precipitation decreased from an average of 0.57 to 0.35 (1979–2018, Ny-Ålesund, Førland et al., 2020). As we did not have data in the reference period of their study, our results can only be compared to rates of increase rather than percentages. The percentage of increase in Førland et al. (2020) translates to an increase of 5.3 mm/year (uncorrected) and 5.6 mm/year (corrected for undercatch) total precipitation during 1979–2018. Our results for only (uncorrected) rainfall 2000–2023 was in the same range. Our results suggest amplifying rainfall trends in the last decades as Aga et al. (2023) found an increase of only 1.3 mm/year for the longer period of 1950–2021 based on downscaled ERA-5 reanalysis data.

Increasing air temperature in the snow season leads to more frequent rain-on-snow events in the Arctic (Groisman et al., 2016) and Svalbard in particular (Peeters et al., 2019; Rinke et al., 2017; Sobota et al., 2020). These events are rare and our statistical approach is not suited for estimating trends of mean monthly rainfall for months which have zero or close to zero rainfall in most years (December–March). However, our analysis indicated that the cumulative sum of rainfall in the months December–March increased between 2000 and 2023.

4.1.3. Snow Cover

A widespread reduction of the snow cover has been observed in the Arctic. In particular, the snow-covered season is shortening by 0.2–0.4 days/year (AMAP, 2017). The changes in the High Arctic are even more pronounced with 0.4–1 days/year (Mohammadzadeh Khani et al., 2022). For Svalbard specifically, Hanssen-Bauer et al. (2019) reported a spatial average shortening of 0.33 days/year for 1958–2017. Locally, shortenings of 0.46 and 1.0 days/year have been observed for 1984–2015 in Barentsburg and Hornsund (both on Svalbard), respectively (Osuch & Wawrzyniak, 2017). van Pelt et al. (2016) estimated a lengthening of the snow-free season in Svalbard by 0.12 days/year. In our study, we found much stronger trends, with a shortening of the spatially closed snow cover of −1.41 ± 0.78 days/year (100%) (Figure 4e) and a lengthening of the completely snow-free period by 0.94 ± 0.46 days/year (100%). To the best of our knowledge, such strong trends have not yet been reported in other studies. One possible explanation may be the specific period studied. Our results were obtained for the years 1999–2023. The extreme changes which we observed in this period cannot be captured when longer periods are considered (such as 1957–2018 in van Pelt et al. (2019)). Furthermore, our site Bayelva is only 1.3 km from the coast and coastal regions tend to show stronger trends (AMAP, 2017).

In most Arctic areas, this shortening of the snow-covered season is mostly happening in spring rather than in autumn (AMAP, 2017). This is in contrast to observations from Canada (Brown et al., 2021) and Svalbard. On Svalbard, melt timing is stable or slightly earlier in most regions, while the delay of the start of snow accumulation is more pronounced with 0.14 ± 0.09 days/year for whole Svalbard 1957–2018 (van Pelt et al., 2019). Even though the average trend in spring melt timing is negligible, van Pelt et al. (2019) observed up to 0.4 days/year shifts toward earlier melt locally. This matches well with observations from Hornsund (0.4 days/year), while the snow in Barentsburg only melted 0.15 days/year earlier between 1984 and 2015 (Osuch & Wawrzyniak, 2017). Similar rates have been reported from Ny-Ålesund with earlier snowmelt by 0.48 ± 0.83 days/year (1993–2013) and 0.4 days/year (1993–2017) (Maturilli et al., 2015, 2019). This agrees very well with our study, as the first snow-free patches appeared −0.43 ± 0.61 days/year (88%) earlier (1999–2023). However, the snow in the village of Ny-Ålesund melts about 2 weeks earlier than at Bayelva (The Norwegian Meteorological Institute (MET Norway), 2024).

Fewer studies focus on snow depth as compared to snow cover duration or snow water equivalent. In particular, recent large scale studies concentrate on snow water equivalent rather than snow depth (Bormann et al., 2018; Hanssen-Bauer et al., 2019; Mudryk et al., 2018; van Pelt et al., 2016). While older studies still show an increase in snowfall and snow depth in northern Eurasia combined with a decrease in the American Arctic (1936–2004) (Callaghan et al., 2011; Mohammadzadeh Khani et al., 2022), the pattern since the 1980s is a general decline of snow depth by 0.002 to 0.04 cm/year (AMAP, 2017). A study on four high Arctic stations in Canada reports

decreasing snow depth at Eureka, Resolute, and Hall Beach in each season of up to 0.28 cm/year while snow depth at Cambridge Bay increased by 0.11 cm/year in winter and 0.19 cm/year in spring (1960–2019, Lam et al., 2023). For Svalbard, changes in maximum annual snow depth have been reported. Maximum annual snow depth decreased by 0.25 and 0.57 cm/year between 1984 and 2016 in Barentsburg and Hornsund, respectively (Osuch & Wawrzyniak, 2017). In their study, the strongest decrease of snow depth has been observed in May and June. The mean monthly snow depth trends at Bayelva ranged from no change in May to a strong decrease of −0.92 ± 0.89 cm/year (99%) in October (1999–2023, Figure 4f). Therefore, we could not confirm decreasing snow depth in May at Bayelva. This is also related to the lacking trend of annual maximum snow depth, which is different to what Osuch and Wawrzyniak (2017) observed. However, for the winter months, our study showed much stronger trends than other studies. Snow cover effects are very local and the data of Ny-Ålesund suggest no change in annual average snow depth since 2010 (Figure D1c).

Despite the large uncertainty, our most recent data of 2010–2023 indicate an accelerated reduction of snow depth for December, January, and February (1.6–2.1 cm/year, Figure 7d and Table 1). The strong changes in these months in recent years likely contributed to the recent stop of active layer warming.

4.2. Active Layer Temperature and Moisture

4.2.1. Active Layer Temperature

Active layer temperature and moisture monitoring is not widespread and, in comparison to climate or permafrost, data are scarce and often short term or unpublished. Literature is mostly limited to changes in active layer thickness or permafrost temperatures (e.g., Smith et al., 2022). Nevertheless, widespread warming of the active layer has been observed in multiple Arctic regions such as Alaska (Wang et al., 2018), the Canadian High Arctic (Farquharson et al., 2019), the western Russian Arctic (Vasiliev et al., 2020) and all of Russia (L. Chen et al., 2021; Streletskiy et al., 2015). The observed rates of temperature change varied widely between cooling of singles sites up to −0.15°C/year and warming of up to 0.3°C/year (ground temperature at 1 m depth at 31 sites in Alaska with at least 5 years of data, Wang et al. (2018)). In the continuous permafrost zone in Russia, the average warming at 0.8 m depth 1975–2016 was 0.033°C/year with a maximum of 0.11 ± 0.02°C/year (L. Chen et al., 2021).

For Svalbard specifically, active layer warming of 0.17 and 0.26°C/year have been observed at UNISCALM in Adventdalen 2000–2014 at 110 and 20 cm depth, respectively (Schuh et al., 2017). We measured warming rates of 0.055 ± 0.067°C/year (91%) near the surface and 0.084 ± 0.048°C/year (99%) at the bottom of the active layer between 1999 and 2023 (Figure 5b). The lower warming rate in our study is likely due to the different observation period. The soil temperature series of Schuh et al. (2017) did not cover the relatively warm year of 1999 nor the recent colder period starting in 2017. We observed stronger warming at the bottom of the active layer (at 94 and 135 cm) as compared to the upper depths. This may have been caused by permafrost degradation at these depths, as they were previously permafrost and are now part of the active layer. To a lesser extent, stronger warming lower down has also been observed for the summer temperature trend at Kaffiøyra Plain (north-western Svalbard) 1975–2014 (Araźny et al., 2016). In Adventdalen, on the other hand, lower depths warmed more slowly than shallow depths (Schuh et al., 2017).

For the most recent period 2010–2023, our results even indicated stable active layer temperatures (Figure 7b). To our knowledge, this recent halting of active layer warming has not yet been reported in the literature. The reduced trend at the lower depths may have been caused by the permafrost table being further away from the measurement depths now. We attribute the change at the soil surface to the very strong reduction in snow depth of October–February in recent years (Figure 7d). At the same time, air temperature of the months January to May showed smaller trends than for 1999–2023. The air temperature trends for 2010–2023 were very uncertain, but showed possible cooling for January and May. While the permafrost at 9 m depth was warming in the recent period, we observed a low warming rate. Single years with little winter snow and low winter temperatures led to decreased temperatures down to the permafrost.

4.2.2. Active Layer Moisture

So far, it is not clear whether Arctic landscapes are wetting or drying as, depending on the topography and permafrost degradation stage, both effects occur (Walvoord & Kurylyk, 2016). While wetting and drying patterns

have been described at the landscape scale (see review by Walvoord and Kurylyk (2016)) and theoretically based on modeling (e.g., Lilhare et al., 2022), we are not aware of recent studies on Arctic soil moisture trends based on subsurface in situ time series. For 1999–2023, we observed a general increase of soil moisture corresponding to warmer temperatures, longer thawed periods, and more annual rainfall (Figure 5e). The effect of active layer temperature on soil moisture is supported by our more recent trend analysis for the period of 2010–2023. The recent stop of active layer warming led to active layer drying at 73 cm depth and above. We observed surface drying in the whole time series, in particular during summer. In addition to possibly reduced rainfall in July, decreased summer soil moisture can be caused by increased evapotranspiration under warmer conditions.

4.3. Freeze/Thaw State

Given recent warming trends in air temperature, changes in the freeze/thaw timing can be expected in Arctic regions. At a large scale, radar remote sensing provides estimates of the frozen or thawed state of the land surface. In their circum-Arctic study based on coarse scale microwave satellite data, X. Chen et al. (2022) estimated a lengthening of the thawed period by 0.25 days/year for the continuous permafrost zone. The thawing started -0.25 days/year earlier while the start of freezing did not show a trend in continuous permafrost (X. Chen et al., 2022). This is in contrast to the study by Li et al. (2023), who found delayed start of freezing in the last 40 years for high-latitude permafrost regions. Both studies used the same data set and identified some Arctic regions which even show earlier freeze-back timing. However, those remote sensing results are hard to compare to ground data because of multiple factors. First, one grid cell contains about 630 km^2. In most Arctic landscapes, this area includes a large portion of water bodies and possibly the sea shore or ice sheets and large spatial heterogeneity. This may be one reason why the agreement of the final data product is less than 70% with ground data at many Arctic sites (Kim et al., 2017). Second, the depth of the freeze-thaw observation is unknown as it depends on the soil moisture. It is rather shallow and can thus only be compared to the highest sensor in our soil profile.

At Bayelva, we found much stronger trends for the lengthening of the thawed period as well as for the earlier start of thawing and, in particular, also for the delayed start of freezing (Figure 6). At the surface, we observed a lengthening of the thawed period of 1.05 ± 0.62 days/year (100%). We observed earlier start of thawing (-1.25 ± 0.61 days/year [100%]) and later start of freezing (0.79 ± 0.73 days/year [96%]). Lower depths showed an even stronger trend toward later freeze-back at Bayelva (Figure 6c). These values are comparable to the timing of freeze-back of the entire active layer. While our numbers are much higher than the estimates based on microwave remote sensing, similar changes have been observed locally. In northern Alaska, the freeze-back date was delayed by almost 2 months in 30 years (1986–2013) (AMAP, 2017), which is within the range of our estimates.

4.4. Permafrost Temperature

Permafrost warming has been observed at many Arctic locations (AMAP, 2017). The average warming rate in the continuous permafrost zone was $0.039 \pm 0.015°C$/year (2007–2016) at the depth of zero annual amplitude (ZAA) (Biskaborn et al., 2019). For Svalbard specifically, a warming trend of $0.09°C$/year has been measured at Janssonhaugen (10 m depth, 1998–2023) (Isaksen et al., 2022a). At Bayelva, we found a warming rate of only $0.014 \pm 0.013°C$/year (95%) at 9 m depth (2010–2023, Figure 7a).

The lower warming rate in our study may be due to three main reasons: First, the permafrost is relatively warm at about $-2.6°C$. Warmer permafrost typically warms at lower rates than cold permafrost (AMAP, 2017) due to smaller thermal gradients and latent heat effects. For soils with high silt or clay content, such as those found at Bayelva, latent heat effects remain significant at temperatures well below $0°C$ which may mask the warming signal even in deeper permafrost layers (Nicolsky & Romanovsky, 2018; Riseborough, 1990). Simulations from Groenke et al. (2023) have indicated that latent heat likely plays a dominant role in the thermal dynamics of the soil at Bayelva.

Second, trends in permafrost temperature depend on the measurement depth (AMAP, 2017). Most trend studies use the ZAA (Biskaborn et al., 2019). Our deepest sensor is at 9 m while the ZAA is expected to be around 20 m (Isaksen et al., 2007, 2022a). Permafrost warming at shallow depth such as 10 m is not linear and extreme conditions show strong effects with a delay of some months. We observed strong permafrost cooling in 2020 and warming in 2016 (Figure 7a). Both events have also been observed on Janssonhaugen at 10 m depth (Isaksen et al., 2022a). The general temperature decrease between 2017 and 2019 at our site has been observed in multiple

boreholes around Svalbard (Christiansen et al., 2020b). This cooling and the cooling of 2020 contributed to the generally small warming trend.

Third, any trend observation strongly depends on the period of study. For example, the study by Groenke et al. (2023) found a warming of 0.02°C/year based on the same data of the Bayelva station but for the period 1999–2020. We suspect that the smaller permafrost temperature trend observed in our study period may be due to the cool temperatures in 2021 and the average temperatures in 2022 in our data set. The upper part of the active layer revealed stable annual temperatures since 2010 (Figure 7b). Given the high interannual variability within the active layer, trends could not be stated with confidence for the 14 year period considered. However, the previously observed warming may have slowed or stopped since 2010. Our analysis suggests that air temperature warming still dominates in most months. However, recent trends for September, October, January, and May air temperature were very uncertain and cooling was possible, in particular in May. We suspect that the strong decrease in early winter snow cover and the reduced winter warming since 2010 are major reasons for the small trend of permafrost temperatures. Such recent developments may not be represented in other studies yet, because so far few studies include the period 2014–2023. On the other hand, this effect may also be site specific. A study of cold permafrost near Station Nord, Greenland, revealed permafrost warming rates of 0.07 and 0.05°C/year in two boreholes at 20 m depth for the recent period of 2014–2021 (Strand et al., 2022). Similarly, a study from the western Russian Arctic found increased permafrost warming in recent years (Vasiliev et al., 2020). Between 2010 and 2020, stable or increasing rates of permafrost warming have been observed at multiple sites of cold (≤ -2°C) permafrost sites (Smith et al., 2022).

5. Conclusion

In summary, our study site in western Svalbard is undergoing significant changes in temperature, rainfall, snow cover, and permafrost conditions. Recent observations suggest a potential slowdown in permafrost warming, highlighting the complex interplay of various climatic factors. September and October stand out with the most substantial air temperature rise since 1999, while recent years exhibit strongest warming in July, August, and November combined with a lack of warming in September, October, January, and May, a deviation not widely reported. Svalbard experiences increased rainfall and exceptionally strong snow cover reduction, marked by both shortened spatially closed cover and lengthened snow-free periods, along with a reduced winter snow thickness. Permafrost warming at the Bayelva permafrost and climate observatory occurs at a slower rate than in other Arctic regions, with recent years even suggesting a potential slowdown, likely influenced by recent winter air cooling periods and reduction of winter snow depth. Active layer warming is evident since 1999, but mostly because of the cold period 1999–2004, while recent years indicate no temperature trend. Overall, soil moisture increases, except at the soil surface, which gets drier in particular in summer. The active layer thawed period exhibits stronger trends in later freeze and earlier thaw timing compared to larger-scale Arctic estimates. Our findings underscore the importance of region-specific analysis in understanding the complex dynamics of Arctic permafrost and climate changes and emphasize the need for continued monitoring and research to assess ongoing trends and their implications.

Appendix A: Spatial Snow Cover Derivation

We estimated the spatial cover fraction of snow at daily resolution within the fenced measurement area based on

- Bayelva snow depth observations (only data source 1998–2007, for comparison processed during the whole period)
- Bayelva noon webcam images manually evaluated (major data source 2007–2023)
- Ny-Ålesund air temperature (used in the gapfilling routine 1998–2023, The Norwegian Meteorological Institute (MET Norway) (2024), https://seklima.met.no/observations)

We used the visually estimated snow cover from webcam images whenever those were available within the period 2007–2023. However, we had some major data gaps and in some years no light source during polar night.

The estimation of spatial snow cover from snow depth was based on the relationship between spatial cover and snow depth in the common period 2007–2023. We applied the following steps:

1. Snow depth data was gapfilled linearly for:

- Gaps up to 3 days length
- Gaps less than 30 days long and snow depth difference before and after less than 2.5 cm
- Maximum of mean daily air temperature <0°C and snow depth before the gap above 2.5 cm
- Maximum hourly air temperature <5°C and snow depth before and after above 20 cm

2. Long gaps with more than 20 cm snow at start are forward-filled with the last measured value until the first hourly air temperature above 5°C
3. The summer (no-snow) value of snow depth sometimes includes vegetation. It was adjusted to zero using the following steps for each year:
   - Compute the average apparent summer snow depth from depth measurements between the latest possible melt end (Day Of Year [DOY] 206) and the following 10 days for each summer individually
   - Set all values to zero which are below (apparent snow depth + 5 cm) for each summer individually
4. Spatial snow cover fraction was estimated linearly from snow depth with separate thresholds for autumn as compared to winter/spring because the spatial snow cover is more homogeneous in autumn:
   - Spring/winter (DOY 1–206): cover = 0 below 2.5 cm and cover = 1 above 20 cm
   - Autumn (DOY 206–365): cover = 0 below 2.5 cm and cover = 1 above 10 cm
5. As the thresholds are not exact, the following corrections were applied:
   - For apparent snowfalls with less than 10 cm of measured additional snow and mean daily air temperature >0°C snow cover is set to the value of the previous day
   - For apparent snowmelt with maximum hourly air temperature <0°C snow cover is set to the value of the previous day
   - During a snowmelt phase, cover = 0 is not reached until the snow depth stops decreasing; all snow cover values between 2.5 cm and the last day of decreasing depth are set to cover = 0.1
6. Calculate annual statistics from the final series for years with sufficient observations:
   - Start of the melting period: day after the last fully snow-covered day of the winter (if <10 missing daily values in spring)
   - End of the melting period: first day of no snow (if <10 missing daily values in spring)
   - Number of snow free days (if <10 missing daily values between spring and autumn)
   - Number of days with full snow cover in space (if <20 missing daily values in whole year)

Appendix B: Derivation of Freeze/Thaw Conditions

Freezing and thawing characteristics at the Bayelva site for each year were estimated based on soil temperature (T_s, °C) at 8 different depths (3, 10, 22, 38, 58, 73, 94, and 135 cm). Each time series contains three ordered levels: (a) warm ($T > 0.2°C$), (b) zero curtain ($-0.5°C < T \leq 0.2°C$, phase change), and (c) cold ($T \leq -0.5°C$). The following procedure was implemented:

1. Fill short gaps (≤ 6 hr) in the Bayelva T_s series with linear interpolation
2. Classify time series of temperature condition based on the two thresholds -0.5 and $0.2°C$; the thresholds to classify the zero curtain are not exactly 0°C to account for measurement uncertainty.
3. Fill gaps in the temperature condition; this was mostly relevant in winters before 2012 which sometimes had larger gaps:
   - fill short breaks (≤ 10 days) if condition before == condition after
   - fill medium breaks (≤ 20 days) if condition before == condition after AND winter (December-June)
   - fill winter breaks starting with cold conditions if Ny-Ålesund mean air temperature (24 hr) $\leq -1.2°C$ (The Norwegian Meteorological Institute (MET Norway) (2024), https://seklima.met.no/observations); Ny-Ålesund air temperature was used as Bayelva air temperature usually had gaps at the same time as soil temperature in early years.
   - fill gaps <24 hr with simple forward fill
4. Smooth the temperature condition to remove periods shorter than 6 hr; these periods are filled with a simple forward fill.
5. Calculate annual statistics from the final series for years with sufficient observations (start/end of thawing/freezing was only calculated if the respective dates were not just after/before a data gap):
   - Number of days with temperatures in the warm, zero curtain, and cold range (calculated from number of hours divided by 24; only calculated for years when the dates of start/end of thawing/freezing could be estimated and when the respective season had no gap of more than 7 days)

- DOY when thawing started in spring (begin of zero curtain conditions)
- DOY when thawing was completed in spring (begin of warm conditions)
- DOY when final freezing started resulting in at least 10 days consecutively cold conditions (last drop to zero curtain conditions)
- DOY when final freezing ended resulting in at least 10 days consecutively cold conditions (last drop to cold conditions); at lower depths, the freezing continues into the new year. In this case the DOY in the new year was added to 365.

Appendix C: Trend Estimates for All Variables

The tables in this section summarize all trend estimates stated in the results and discussed in relation to literature findings. For each trend estimate, we provide the median of all samples. The uncertainty is stated as symmetrized 90% confidence interval and the posterior probability that the trend direction is the same as the direction of the median is given in brackets. Numbers above 90% indicate high confidence in the trend estimate (black in the tables), between 80% and 90%, we interpret the results as indication of a certain trend direction (dark gray), below 80%, the uncertainty is high and the values should not be over-interpreted (light gray).

Table C1
Trend Estimates for Snow Characteristics Between October 1998 and December 2023; DOY: Day Of Year

DOY start melting, first snow-free patch	days/year	-0.43 ± 0.61 (87.8%)
DOY end melting, all snow gone	days/year	-0.39 ± 0.64 (84.7%)
Nr days with 100% spatial snow cover	days/year	-1.41 ± 0.78 (99.9%)
Nr days with 0% spatial snow cover	days/year	0.94 ± 0.46 (100.0%)
Nr days with more than 50% spatial snow cover	days/year	-0.60 ± 0.80 (89.7%)
Nr days with more than 90% spatial snow cover	days/year	-0.72 ± 0.78 (94.1%)
Annual maximum snow depth	cm/year	0.10 ± 1.00 (56.4%)
DOY of maximum snow depth	days/year	0.35 ± 0.45 (91.0%)

Note. Trend estimates provided as median of all samples ± symmetrized 90% confidence interval (posterior probability that the trend direction is the same as the direction of the median); trend estimates with high confidence are shown in black, medium confidence in dark gray, and low confidence in light gray.

Table C2

Trend Estimates for Active Layer Temperature Between October 1998 and December 2023 (Top) and Between January 2010 and December 2023 (Bottom); Winter Is Defined as January–March Representing the Three Coldest Months, Summer as June–August

	3 cm °C/year	10 cm °C/year	22 cm °C/year	38 cm °C/year	58 cm °C/year	73 cm °C/year	94 cm °C/year	135 cm °C/year
October 1998 to December 2023								
Annual	0.054 ± 0.063 (92.7%)	0.055 ± 0.067 (91.1%)	0.052 ± 0.066 (89.8%)	0.056 ± 0.065 (92.6%)	0.064 ± 0.065 (94.3%)	0.060 ± 0.064 (93.3%)	0.084 ± 0.063 (98.3%)	0.084 ± 0.048 (99.5%)
Summer	0.076 ± 0.053 (98.5%)	0.079 ± 0.053 (99.1%)	0.063 ± 0.048 (98.0%)	0.067 ± 0.051 (97.9%)	0.074 ± 0.044 (99.8%)	0.082 ± 0.044 (99.9%)	0.111 ± 0.036 (100.0%)	0.082 ± 0.026 (100.0%)
Winter	0.056 ± 0.149 (74.0%)	0.067 ± 0.157 (75.7%)	0.062 ± 0.151 (74.6%)	0.072 ± 0.148 (78.0%)	0.080 ± 0.147 (83.2%)	0.072 ± 0.134 (82.5%)	0.090 ± 0.125 (88.4%)	0.105 ± 0.101 (95.6%)
January	0.041 ± 0.149 (68.3%)	0.051 ± 0.143 (73.1%)	0.050 ± 0.137 (73.1%)	0.065 ± 0.137 (78.9%)	0.076 ± 0.132 (82.9%)	0.076 ± 0.126 (84.5%)	0.090 ± 0.114 (90.6%)	0.103 ± 0.086 (97.3%)
February	0.051 ± 0.156 (71.3%)	0.052 ± 0.162 (70.8%)	0.052 ± 0.160 (71.2%)	0.059 ± 0.156 (73.9%)	0.063 ± 0.153 (76.0%)	0.057 ± 0.148 (74.1%)	0.078 ± 0.137 (83.0%)	0.099 ± 0.113 (92.8%)
March	0.080 ± 0.167 (78.7%)	0.088 ± 0.173 (80.2%)	0.085 ± 0.168 (80.4%)	0.092 ± 0.164 (82.4%)	0.092 ± 0.157 (83.8%)	0.079 ± 0.148 (81.3%)	0.102 ± 0.140 (89.0%)	0.108 ± 0.117 (93.8%)
April	0.121 ± 0.129 (93.6%)	0.113 ± 0.130 (92.4%)	0.111 ± 0.130 (92.2%)	0.112 ± 0.131 (91.7%)	0.114 ± 0.131 (92.2%)	0.097 ± 0.128 (89.4%)	0.120 ± 0.123 (94.4%)	0.116 ± 0.109 (96.0%)
May	0.095 ± 0.082 (97.1%)	0.091 ± 0.083 (96.2%)	0.093 ± 0.084 (96.5%)	0.095 ± 0.081 (97.1%)	0.101 ± 0.082 (97.6%)	0.085 ± 0.080 (95.7%)	0.118 ± 0.078 (99.1%)	0.111 ± 0.076 (99.0%)
June	0.113 ± 0.082 (98.7%)	0.086 ± 0.060 (98.7%)	0.065 ± 0.048 (98.5%)	0.051 ± 0.036 (98.9%)	0.051 ± 0.033 (99.5%)	0.038 ± 0.032 (97.2%)	0.076 ± 0.037 (100.0%)	0.066 ± 0.041 (99.6%)
July	0.088 ± 0.064 (98.6%)	0.094 ± 0.067 (98.9%)	0.086 ± 0.068 (97.9%)	0.077 ± 0.073 (95.9%)	0.097 ± 0.070 (98.6%)	0.092 ± 0.063 (99.0%)	0.112 ± 0.047 (100.0%)	0.071 ± 0.026 (100.0%)
August	0.072 ± 0.038 (99.8%)	0.083 ± 0.039 (100.0%)	0.081 ± 0.037 (100.0%)	0.090 ± 0.036 (100.0%)	0.107 ± 0.038 (100.0%)	0.118 ± 0.041 (100.0%)	0.158 ± 0.040 (100.0%)	0.125 ± 0.029 (100.0%)
September	0.070 ± 0.045 (99.3%)	0.052 ± 0.036 (98.8%)	0.058 ± 0.032 (99.7%)	0.048 ± 0.029 (99.5%)	0.069 ± 0.024 (100.0%)	0.065 ± 0.023 (100.0%)	0.089 ± 0.018 (100.0%)	0.081 ± 0.014 (100.0%)
October	0.014 ± 0.054 (66.9%)	0.019 ± 0.041 (78.3%)	0.029 ± 0.034 (92.8%)	0.027 ± 0.024 (97.0%)	0.023 ± 0.014 (99.8%)	0.013 ± 0.010 (99.0%)	0.028 ± 0.009 (100.0%)	0.036 ± 0.009 (100.0%)
November	0.007 ± 0.067 (56.9%)	0.012 ± 0.059 (64.1%)	0.016 ± 0.054 (69.1%)	0.022 ± 0.046 (79.3%)	0.024 ± 0.036 (87.2%)	0.004 ± 0.021 (74.0%)	0.014 ± 0.012 (99.6%)	0.036 ± 0.018 (100.0%)
December	0.025 ± 0.111 (64.5%)	0.027 ± 0.105 (66.4%)	0.021 ± 0.099 (63.6%)	0.037 ± 0.091 (75.0%)	0.046 ± 0.087 (81.2%)	0.045 ± 0.077 (83.8%)	0.060 ± 0.064 (94.0%)	0.068 ± 0.043 (99.3%)
January 2010 to December 2023								
Annual	−0.009 ± 0.105 (56.1%)	0.005 ± 0.107 (53.4%)	−0.001 ± 0.109 (50.7%)	0.000 ± 0.106 (50.1%)	0.004 ± 0.107 (52.1%)	0.007 ± 0.099 (54.4%)	0.007 ± 0.095 (55.4%)	0.016 ± 0.081 (62.7%)
Summer	0.104 ± 0.130 (90.5%)	0.111 ± 0.121 (93.6%)	0.096 ± 0.117 (92.1%)	0.084 ± 0.106 (90.8%)	0.083 ± 0.097 (91.8%)	0.078 ± 0.086 (93.2%)	0.070 ± 0.070 (95.2%)	0.061 ± 0.044 (98.5%)
Winter	−0.108 ± 0.297 (73.9%)	−0.053 ± 0.314 (61.0%)	−0.057 ± 0.315 (62.4%)	−0.052 ± 0.308 (63.0%)	−0.053 ± 0.294 (62.2%)	−0.043 ± 0.280 (60.2%)	−0.038 ± 0.242 (60.8%)	−0.022 ± 0.194 (58.5%)
January	−0.070 ± 0.274 (66.6%)	−0.062 ± 0.262 (65.3%)	−0.054 ± 0.261 (63.7%)	−0.038 ± 0.253 (60.1%)	−0.028 ± 0.253 (57.8%)	−0.014 ± 0.244 (54.1%)	−0.009 ± 0.225 (52.6%)	0.001 ± 0.161 (50.4%)
February	−0.065 ± 0.313 (64.3%)	−0.056 ± 0.312 (62.2%)	−0.060 ± 0.309 (63.5%)	−0.071 ± 0.298 (65.9%)	−0.070 ± 0.280 (66.7%)	−0.064 ± 0.263 (66.8%)	−0.066 ± 0.239 (68.1%)	−0.049 ± 0.188 (68.0%)
March	−0.252 ± 0.400 (86.0%)	−0.006 ± 0.432 (50.9%)	−0.001 ± 0.425 (50.2%)	−0.002 ± 0.402 (50.2%)	−0.007 ± 0.382 (51.3%)	−0.004 ± 0.366 (50.7%)	−0.006 ± 0.322 (51.2%)	−0.010 ± 0.245 (52.5%)
April	0.201 ± 0.360 (82.4%)	0.080 ± 0.342 (65.4%)	0.078 ± 0.332 (65.5%)	0.075 ± 0.326 (65.3%)	0.068 ± 0.318 (64.5%)	0.062 ± 0.313 (63.6%)	0.054 ± 0.305 (62.0%)	0.032 ± 0.257 (58.6%)

Table C2
Continued

	3 cm °C/year	10 cm °C/year	22 cm °C/year	38 cm °C/year	58 cm °C/year	73 cm °C/year	94 cm °C/year	135 cm °C/year
May	−0.021 ± 0.155 (58.9%)	−0.003 ± 0.158 (51.3%)	−0.003 ± 0.154 (51.3%)	0.009 ± 0.159 (54.0%)	0.015 ± 0.160 (56.0%)	0.022 ± 0.159 (59.3%)	0.025 ± 0.161 (60.3%)	0.034 ± 0.155 (64.6%)
June	0.034 ± 0.183 (62.5%)	0.042 ± 0.134 (70.5%)	0.024 ± 0.106 (65.8%)	0.021 ± 0.062 (72.9%)	0.013 ± 0.042 (70.2%)	0.009 ± 0.039 (66.2%)	0.013 ± 0.043 (69.1%)	0.016 ± 0.058 (68.0%)
July	0.143 ± 0.186 (90.3%)	0.140 ± 0.186 (90.0%)	0.109 ± 0.194 (83.4%)	0.093 ± 0.201 (79.1%)	0.087 ± 0.186 (78.5%)	0.080 ± 0.162 (80.8%)	0.059 ± 0.115 (81.3%)	0.044 ± 0.053 (91.5%)
August	0.139 ± 0.108 (97.9%)	0.149 ± 0.105 (98.4%)	0.143 ± 0.103 (98.3%)	0.145 ± 0.100 (98.7%)	0.141 ± 0.095 (98.9%)	0.140 ± 0.090 (99.0%)	0.132 ± 0.086 (99.1%)	0.120 ± 0.063 (99.8%)
September	0.029 ± 0.089 (71.5%)	0.036 ± 0.077 (78.4%)	0.039 ± 0.074 (81.5%)	0.044 ± 0.069 (85.7%)	0.046 ± 0.066 (87.8%)	0.049 ± 0.061 (91.0%)	0.053 ± 0.056 (93.8%)	0.055 ± 0.041 (98.5%)
October	−0.015 ± 0.133 (58.1%)	−0.025 ± 0.095 (68.0%)	−0.011 ± 0.073 (60.8%)	0.000 ± 0.044 (50.1%)	0.005 ± 0.031 (61.9%)	0.005 ± 0.029 (59.7%)	0.008 ± 0.028 (69.7%)	0.010 ± 0.020 (81.3%)
November	0.044 ± 0.162 (68.7%)	0.019 ± 0.144 (59.4%)	0.009 ± 0.130 (54.8%)	−0.002 ± 0.101 (51.5%)	−0.009 ± 0.063 (59.9%)	−0.005 ± 0.033 (61.4%)	−0.001 ± 0.015 (55.1%)	0.004 ± 0.009 (79.7%)
December	−0.078 ± 0.296 (67.3%)	−0.076 ± 0.269 (68.7%)	−0.067 ± 0.254 (67.5%)	−0.054 ± 0.222 (66.4%)	−0.038 ± 0.208 (62.9%)	−0.023 ± 0.180 (58.9%)	−0.006 ± 0.146 (53.1%)	0.017 ± 0.085 (64.3%)

Note. Trend estimates provided as median of all samples ± symmetrized 90% confidence interval (posterior probability that the trend direction is the same as the direction of the median); trend estimates with high confidence are shown in black, medium confidence in dark gray, and low confidence in light gray.

Table C3

Trend Estimates for Active Layer Soil Moisture Between October 1998 and December 2023 (Top) and Between January 2010 and December 2023 (Bottom); Winter Is Defined as January–March Representing the Three Coldest Months, Summer as June–August

	3 cm vol %/year	10 cm vol %/year	22 cm vol %/year	38 cm vol %/year	58 cm vol %/year	73 cm vol %/year	94 cm vol %/year
October 1998 to December 2023							
Annual	−0.27 ± 0.08 (100.0%)	0.18 ± 0.09 (99.8%)	0.13 ± 0.09 (98.6%)	0.04 ± 0.09 (79.0%)	0.12 ± 0.12 (95.4%)	0.15 ± 0.14 (95.6%)	0.18 ± 0.08 (99.9%)
Summer	−0.36 ± 0.12 (100.0%)	0.07 ± 0.14 (81.8%)	0.10 ± 0.11 (91.0%)	0.04 ± 0.14 (71.1%)	0.12 ± 0.13 (94.2%)	0.16 ± 0.18 (93.5%)	0.25 ± 0.10 (100.0%)
Winter	−0.21 ± 0.12 (99.5%)	0.17 ± 0.08 (99.9%)	0.11 ± 0.10 (96.6%)	−0.01 ± 0.12 (56.0%)	0.08 ± 0.17 (78.2%)	0.18 ± 0.21 (92.6%)	0.06 ± 0.10 (84.0%)
January	−0.25 ± 0.14 (99.8%)	0.17 ± 0.09 (99.8%)	0.10 ± 0.10 (94.6%)	−0.02 ± 0.12 (60.6%)	0.08 ± 0.19 (76.5%)	0.22 ± 0.27 (91.2%)	0.06 ± 0.12 (79.2%)
February	−0.21 ± 0.14 (99.4%)	0.17 ± 0.09 (99.8%)	0.10 ± 0.11 (93.8%)	−0.02 ± 0.12 (60.9%)	0.06 ± 0.17 (72.8%)	0.14 ± 0.20 (88.2%)	0.04 ± 0.10 (79.2%)
March	−0.18 ± 0.12 (99.5%)	0.17 ± 0.07 (100.0%)	0.11 ± 0.07 (99.2%)	0.00 ± 0.08 (51.5%)	0.08 ± 0.12 (86.5%)	0.17 ± 0.14 (97.6%)	0.06 ± 0.07 (90.7%)
April	−0.17 ± 0.11 (99.4%)	0.18 ± 0.06 (100.0%)	0.12 ± 0.06 (99.8%)	0.01 ± 0.07 (55.8%)	0.09 ± 0.10 (93.6%)	0.18 ± 0.10 (99.8%)	0.07 ± 0.06 (97.1%)
May	−0.14 ± 0.10 (98.9%)	0.19 ± 0.07 (100.0%)	0.13 ± 0.06 (100.0%)	−0.00 ± 0.07 (54.7%)	0.10 ± 0.08 (97.5%)	0.18 ± 0.08 (99.9%)	0.07 ± 0.05 (98.3%)
June	−0.09 ± 0.20 (76.6%)	0.50 ± 0.29 (99.6%)	0.43 ± 0.26 (99.6%)	0.15 ± 0.21 (88.6%)	0.20 ± 0.14 (98.9%)	0.20 ± 0.11 (99.6%)	0.07 ± 0.05 (98.0%)
July	−0.50 ± 0.16 (100.0%)	−0.12 ± 0.10 (97.9%)	0.00 ± 0.10 (52.0%)	0.05 ± 0.14 (71.5%)	0.24 ± 0.16 (99.2%)	0.33 ± 0.23 (99.0%)	0.35 ± 0.14 (100.0%)
August	−0.44 ± 0.15 (100.0%)	−0.10 ± 0.12 (92.8%)	−0.01 ± 0.11 (54.4%)	0.01 ± 0.15 (53.7%)	0.07 ± 0.10 (89.3%)	−0.04 ± 0.12 (71.9%)	0.35 ± 0.13 (100.0%)
September	−0.11 ± 0.18 (84.7%)	0.46 ± 0.26 (99.7%)	0.29 ± 0.17 (99.7%)	0.27 ± 0.13 (99.9%)	0.21 ± 0.11 (99.8%)	0.00 ± 0.08 (52.5%)	0.31 ± 0.11 (100.0%)
October	−0.35 ± 0.17 (99.9%)	0.31 ± 0.25 (97.9%)	0.31 ± 0.31 (95.0%)	0.37 ± 0.31 (97.3%)	0.38 ± 0.23 (99.6%)	0.19 ± 0.17 (97.0%)	0.39 ± 0.08 (100.0%)
November	−0.36 ± 0.12 (100.0%)	0.18 ± 0.10 (99.6%)	0.12 ± 0.16 (88.4%)	0.04 ± 0.27 (59.4%)	0.28 ± 0.29 (94.4%)	0.44 ± 0.36 (97.4%)	0.36 ± 0.13 (100.0%)
December	−0.29 ± 0.12 (100.0%)	0.18 ± 0.07 (100.0%)	0.10 ± 0.10 (93.9%)	−0.04 ± 0.16 (65.8%)	0.17 ± 0.26 (86.5%)	0.40 ± 0.40 (94.8%)	0.17 ± 0.16 (96.0%)
January 2010 to December 2023							
Annual	−0.479 ± 0.284 (99.4%)	−0.128 ± 0.247 (81.5%)	−0.137 ± 0.205 (87.8%)	−0.059 ± 0.207 (68.9%)	−0.184 ± 0.261 (88.9%)	−0.227 ± 0.256 (93.6%)	0.061 ± 0.205 (69.7%)
Summer	−0.204 ± 0.323 (87.1%)	−0.075 ± 0.330 (66.5%)	0.137 ± 0.258 (82.1%)	0.187 ± 0.317 (84.6%)	−0.055 ± 0.354 (61.4%)	−0.061 ± 0.374 (61.2%)	0.070 ± 0.279 (68.0%)
Winter	−0.768 ± 0.624 (99.3%)	−0.123 ± 0.259 (79.9%)	−0.117 ± 0.284 (77.9%)	−0.062 ± 0.303 (65.0%)	−0.230 ± 0.430 (83.5%)	−0.394 ± 0.606 (87.8%)	0.070 ± 0.192 (74.0%)
January	−0.456 ± 0.334 (98.9%)	−0.091 ± 0.169 (82.3%)	−0.007 ± 0.186 (52.6%)	0.024 ± 0.198 (58.1%)	0.010 ± 0.353 (51.9%)	−0.041 ± 0.649 (54.7%)	0.173 ± 0.246 (88.2%)
February	−0.865 ± 0.668 (99.3%)	−0.179 ± 0.302 (85.8%)	−0.171 ± 0.341 (82.1%)	−0.105 ± 0.347 (70.9%)	−0.258 ± 0.466 (83.9%)	−0.361 ± 0.559 (87.5%)	0.096 ± 0.150 (86.3%)
March	−0.396 ± 0.393 (96.7%)	−0.056 ± 0.170 (72.0%)	−0.048 ± 0.199 (66.9%)	−0.025 ± 0.221 (57.8%)	−0.125 ± 0.290 (77.5%)	−0.210 ± 0.331 (86.3%)	0.135 ± 0.104 (97.8%)
April	−0.634 ± 0.595 (97.9%)	−0.022 ± 0.164 (59.6%)	−0.009 ± 0.169 (53.7%)	0.017 ± 0.186 (56.9%)	−0.050 ± 0.223 (65.3%)	−0.110 ± 0.251 (78.0%)	0.159 ± 0.091 (99.4%)

Table C3
Continued

	3 cm vol %/year	10 cm vol %/year	22 cm vol %/year	38 cm vol %/year	58 cm vol %/year	73 cm vol %/year	94 cm vol %/year
May	−0.341 ± 0.345 (95.7%)	−0.008 ± 0.149 (53.9%)	0.049 ± 0.119 (76.2%)	0.069 ± 0.150 (78.5%)	0.033 ± 0.158 (64.6%)	−0.013 ± 0.162 (55.4%)	0.170 ± 0.093 (99.4%)
June	−0.002 ± 0.514 (50.2%)	0.355 ± 0.870 (76.2%)	0.413 ± 0.827 (80.2%)	0.342 ± 0.684 (80.7%)	0.221 ± 0.370 (85.2%)	0.028 ± 0.110 (68.0%)	0.189 ± 0.096 (99.5%)
July	−0.421 ± 0.423 (95.1%)	−0.186 ± 0.335 (83.7%)	0.143 ± 0.327 (77.7%)	0.280 ± 0.445 (86.3%)	0.096 ± 0.516 (62.5%)	0.230 ± 0.677 (72.7%)	0.186 ± 0.459 (75.6%)
August	−0.111 ± 0.459 (66.6%)	−0.097 ± 0.358 (68.5%)	0.165 ± 0.327 (80.5%)	0.372 ± 0.328 (96.8%)	0.111 ± 0.212 (81.8%)	0.140 ± 0.297 (79.2%)	0.156 ± 0.240 (86.6%)
September	−0.173 ± 0.523 (71.7%)	−0.025 ± 0.341 (55.2%)	0.205 ± 0.279 (89.3%)	0.331 ± 0.193 (99.4%)	0.132 ± 0.108 (97.2%)	0.166 ± 0.207 (91.0%)	0.261 ± 0.181 (98.8%)
October	−0.561 ± 0.533 (96.3%)	−0.478 ± 0.733 (86.8%)	−0.351 ± 0.800 (77.8%)	−0.101 ± 0.717 (59.6%)	−0.064 ± 0.395 (61.2%)	0.048 ± 0.240 (63.5%)	0.025 ± 0.203 (58.4%)
November	−0.374 ± 0.304 (98.1%)	−0.040 ± 0.283 (60.0%)	0.028 ± 0.532 (53.7%)	0.019 ± 0.759 (51.7%)	−0.012 ± 0.871 (51.0%)	−0.138 ± 0.738 (62.9%)	0.232 ± 0.448 (81.9%)
December	−0.394 ± 0.371 (97.2%)	−0.022 ± 0.221 (57.0%)	0.057 ± 0.271 (65.0%)	0.060 ± 0.328 (63.1%)	−0.028 ± 0.797 (52.4%)	0.083 ± 1.258 (54.5%)	0.262 ± 0.555 (79.5%)

Note. Trend estimates provided as median of all samples ± symmetrized 90% confidence interval (posterior probability that the trend direction is the same as the direction of the median); trend estimates with high confidence are shown in black, medium confidence in dark gray, and low confidence in light gray.

Table C4
Trend Estimates for Freeze/Thaw Timing at Different Depths Between October 1998 and December 2023; DOY: Day Of Year

	Nr days thawed days/year	Nr days at 0°C days/year	Nr days frozen days/year	DOY start thawing days/year	DOY start freezing days/year
3 cm	1.05 ± 0.62 (99.7%)	0.50 ± 0.94 (81.7%)	−1.37 ± 1.07 (98.5%)	−1.25 ± 0.61 (100.0%)	0.79 ± 0.73 (96.2%)
10 cm	1.22 ± 0.66 (99.7%)	−0.69 ± 1.50 (78.0%)	−0.08 ± 1.54 (53.5%)	−0.61 ± 0.59 (95.7%)	0.53 ± 0.74 (88.1%)
22 cm	1.31 ± 0.63 (99.8%)	−0.83 ± 1.71 (79.7%)	−0.47 ± 1.82 (66.6%)	−0.55 ± 0.60 (93.4%)	0.82 ± 0.76 (96.2%)
38 cm	1.23 ± 0.66 (99.8%)	−1.20 ± 1.91 (85.2%)	−0.07 ± 2.02 (52.8%)	−0.41 ± 0.68 (85.2%)	0.86 ± 0.83 (95.8%)
58 cm	1.47 ± 0.59 (100.0%)	−0.57 ± 1.66 (73.8%)	−0.11 ± 2.02 (53.5%)	−0.47 ± 0.63 (88.2%)	1.01 ± 0.81 (97.9%)
73 cm	1.31 ± 0.66 (100.0%)	−0.77 ± 1.59 (79.7%)	−0.21 ± 2.00 (56.8%)	−0.36 ± 0.65 (82.0%)	0.94 ± 0.86 (96.3%)
94 cm	2.45 ± 0.89 (100.0%)	−0.63 ± 1.45 (77.7%)	−1.29 ± 1.86 (86.3%)	−0.96 ± 0.69 (98.8%)	1.40 ± 0.83 (99.7%)
135 cm	3.85 ± 0.92 (100.0%)	0.82 ± 1.40 (83.5%)	−3.58 ± 1.87 (99.9%)	−1.24 ± 0.73 (99.8%)	1.64 ± 1.11 (99.0%)

Note. Trend estimates provided as median of all samples ± symmetrized 90% confidence interval (posterior probability that the trend direction is the same as the direction of the median); trend estimates with high confidence are shown in black, medium confidence in dark gray, and low confidence in light gray.

Table C5

Trend Estimates for Permafrost Temperature at Different Depths Between January 2010 and December 2023; Winter Is Defined as January–March Representing the Three Coldest Months, Summer Is June–August

	250 cm °C/year	350 cm °C/year	550 cm °C/year	750 cm °C/year	900 cm °C/year
Annual	0.007 ± 0.051 (59.2%)	0.016 ± 0.034 (77.7%)	0.014 ± 0.019 (87.9%)	0.016 ± 0.018 (92.6%)	0.014 ± 0.013 (95.0%)
Summer	0.006 ± 0.043 (58.3%)	0.005 ± 0.042 (57.4%)	0.014 ± 0.029 (77.8%)	0.017 ± 0.023 (89.4%)	0.013 ± 0.016 (91.7%)
Winter	−0.012 ± 0.092 (57.8%)	0.012 ± 0.038 (69.6%)	0.007 ± 0.016 (79.5%)	0.009 ± 0.017 (83.3%)	0.009 ± 0.013 (87.0%)
January	0.035 ± 0.068 (80.1%)	0.023 ± 0.022 (95.6%)	0.012 ± 0.016 (89.9%)	0.013 ± 0.018 (88.4%)	0.012 ± 0.014 (92.1%)
February	−0.015 ± 0.091 (61.1%)	0.015 ± 0.040 (73.2%)	0.008 ± 0.015 (82.2%)	0.009 ± 0.016 (81.6%)	0.009 ± 0.013 (87.9%)
March	−0.037 ± 0.139 (67.8%)	0.001 ± 0.059 (50.7%)	0.007 ± 0.015 (79.5%)	0.011 ± 0.016 (88.2%)	0.010 ± 0.013 (89.8%)
April	−0.041 ± 0.135 (69.8%)	−0.001 ± 0.073 (51.2%)	0.011 ± 0.019 (84.3%)	0.015 ± 0.016 (94.1%)	0.014 ± 0.012 (96.2%)
May	−0.025 ± 0.100 (67.4%)	−0.000 ± 0.071 (50.3%)	0.012 ± 0.024 (79.0%)	0.015 ± 0.018 (91.9%)	0.013 ± 0.013 (94.7%)
June	−0.013 ± 0.056 (64.6%)	−0.001 ± 0.055 (50.8%)	0.013 ± 0.028 (78.1%)	0.016 ± 0.021 (90.8%)	0.013 ± 0.015 (93.1%)
July	0.006 ± 0.036 (61.7%)	0.005 ± 0.039 (58.1%)	0.013 ± 0.029 (76.6%)	0.017 ± 0.025 (87.5%)	0.013 ± 0.017 (89.7%)
August	0.028 ± 0.026 (96.0%)	0.013 ± 0.028 (78.2%)	0.014 ± 0.027 (81.0%)	0.018 ± 0.025 (87.6%)	0.014 ± 0.018 (90.1%)
September	0.032 ± 0.018 (99.6%)	0.019 ± 0.021 (93.3%)	0.015 ± 0.024 (85.2%)	0.018 ± 0.024 (88.9%)	0.014 ± 0.018 (90.5%)
October	0.035 ± 0.018 (99.8%)	0.023 ± 0.018 (97.9%)	0.017 ± 0.022 (90.5%)	0.019 ± 0.022 (91.7%)	0.015 ± 0.017 (92.5%)
November	0.031 ± 0.017 (99.7%)	0.027 ± 0.017 (99.3%)	0.018 ± 0.019 (93.6%)	0.019 ± 0.020 (93.1%)	0.017 ± 0.017 (94.9%)
December	0.021 ± 0.037 (83.2%)	0.026 ± 0.016 (99.2%)	0.018 ± 0.017 (95.5%)	0.019 ± 0.018 (95.5%)	0.017 ± 0.015 (96.4%)

Note. Trend estimates provided as median of all samples ± symmetrized 90% confidence interval (posterior probability that the trend direction is the same as the direction of the median); trend estimates with high confidence are shown in black, medium confidence in dark gray, and low confidence in light gray.

Appendix D: Results of Bayelva in Comparison to Ny-Ålesund

As the Ny-Ålesund meteorological station data is freely available at The Norwegian Meteorological Institute (MET Norway) (2024), we analyzed this data with the same method as our Bayelva data. The village Ny-Ålesund is about 2 km from Bayelva at the coast. Air temperature trends can be validly compared over the entire period from 1999 to 2023 (Figure D1a). However, due to the lack of snow depth data at Ny-Ålesund from 1979 to 2009, we cannot compare this variable for our main study period of 1998–2023. Therefore, Figure D1c only includes data from 2010 to 2023. For precipitation, the comparison is more complex as we only observe rainfall and not total precipitation like in Ny-Ålesund (Figure D1b).

As shown in Figure D1a, the air temperature trends agree well for Bayelva and Ny-Ålesund. However, the absolute temperatures differ with Bayelva being roughly 1°C colder. The weather stations at Ny-Ålesund and Bayelva, although geographically proximate, exhibit distinctly different climatic and environmental characteristics. For example, Ny-Ålesund experiences substantial human influence from the village, while Bayelva is influenced by natural factors such as proximity to the Brøggerbreen glacier, leading to cold air events. Rainfall and total precipitation trends cannot be compared directly (Figure D1b). However, our analysis suggests that total precipitation shows a slightly stronger increase than rainfall. However, the rain to snow ratio likely differs between the two stations. This is indicated by the substantial differences in snow cover. At Bayelva, the snow cover is considerably thicker and persists longer into the season, affecting both albedo and local radiation balance differently compared to Ny-Ålesund. Snow depth at Bayelva shows a decreasing trend since 2010 (in particular in early winter), while the generally much thinner cover at Ny-Ålesund seems to be stable (Figure D1c).
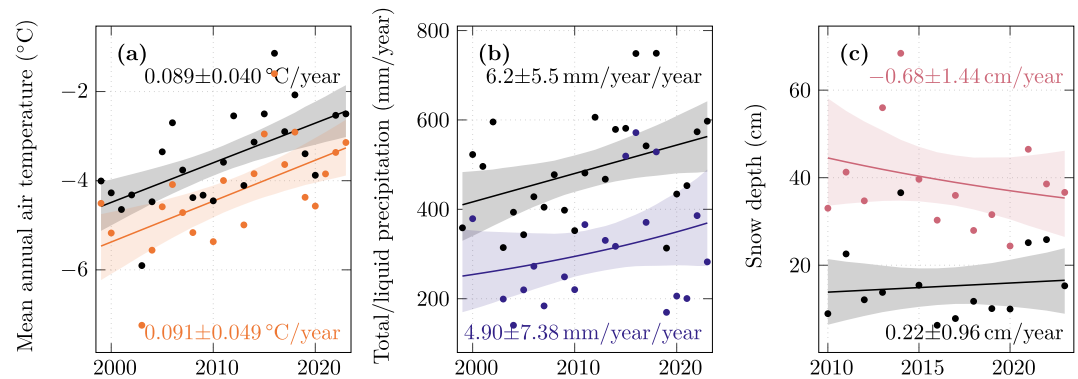
Figure D1. Trends in annual values at Ny-Ålesund (black) compared to Bayelva (colored) for 1999–2023 (air temperature (a) and precipitation (b)) and 2010–2023 (snow depth (c)) calculated with the same method aggregated from daily data from The Norwegian Meteorological Institute (MET Norway) (2024). Please note that at Bayelva only liquid precipitation (rain) is measured while the Ny-Ålesund data contains total precipitation.

Data Availability Statement

All data used in the presented analysis is published as a supplement to this article on Pangaea (Grünberg et al., 2024a). Data of future years will be included within the collection (Grünberg et al., 2024b).

References

Aga, J., Piermattei, L., Girod, L., Aalstad, K., Eiken, T., Kääb, A., & Westermann, S. (2023). Coastal retreat rates of high-Arctic rock cliffs on Brøgger peninsula, Svalbard, accelerate during the past decade. *EGUsphere*, *2023*, 1–24. https://doi.org/10.5194/egusphere-2023-321

AMAP. (2017). Snow, Water, Ice and Permafrost in the Arctic (SWIPA) 2017. Retrieved from https://www.amap.no/documents/download/2987/inline

Araźny, A., Przybylak, R., & Kejna, M. (2016). Ground temperature changes on the Kaffiøyra Plain (Spitsbergen) in the summer seasons, 1975–2014. *Polish Polar Research*, *37*(1), 1–21. Retrieved from https://bibliotekanauki.pl/articles/2046859

Bintanja, R., & Andry, O. (2017). Towards a rain-dominated Arctic. *Nature Climate Change*, *7*(4), 263–267. https://doi.org/10.1038/nclimate3240

Biskaborn, B. K., Smith, S. L., Noetzli, J., Matthes, H., Vieira, G., Streletskiy, D. A., et al. (2019). Permafrost is warming at a global scale. *Nature Communications*, *10*(264), 264. ISSN: 2041-1723. https://doi.org/10.1038/s41467-018-08240-4

Boike, J., Ippisch, O., Overduin, P. P., Hagedorn, B., & Roth, K. (2008). Water, heat and solute dynamics of a mud boil, Spitsbergen. *Geomorphology*, *95*(1), 61–73. https://doi.org/10.1016/j.geomorph.2006.07.033

Boike, J., Juszak, I., Lange, S., Chadburn, S., Burke, E., Overduin, P. P., et al. (2018). A 20-year record (1998–2017) of permafrost, active layer and meteorological conditions at a high Arctic permafrost research site (Bayelva, Spitsbergen). *Earth System Science Data*, *10*(1), 355–390. https://doi.org/10.5194/essd-10-355-2018

Boike, J., Roth, K., & Ippisch, O. (2003). Seasonal snow cover on frozen ground: Energy balance calculations of a permafrost site near Ny-Ålesund, Spitsbergen. *Journal of Geophysical Research*, *108*(D2), 8163. https://doi.org/10.1029/2001JD000939

Bormann, K. J., Brown, R. D., Derksen, C., & Painter, T. H. (2018). Estimating snow-cover trends from space. *Nature Climate Change*, *8*(11), 924–928. https://doi.org/10.1038/s41558-018-0318-3

Brown, R. D., Smith, C., Derksen, C., & Mudryk, L. (2021). Canadian in situ snow cover trends for 1955–2017 including an assessment of the impact of automation. *Atmosphere-Ocean*, *59*(2), 77–92. https://doi.org/10.1080/07055900.2021.1911781

Callaghan, T. V., Johansson, M., Brown, R. D., Groisman, P. Y., Labba, N., Radionov, V., et al. (2011). The changing face of Arctic snow cover: A synthesis of observed and projected changes. *Ambio*, *40*(1), 17–31. https://doi.org/10.1007/s13280-011-0212-y

Calonne, N., Flin, F., Morin, S., Lesaffre, B., du Roscoat, S. R., & Geindreau, C. (2011). Numerical and experimental investigations of the effective thermal conductivity of snow. *Geophysical Research Letters*, *38*(23), L23501. https://doi.org/10.1029/2011GL049234

Capretto, T., Piho, C., Kumar, R., Westfall, J., Yarkoni, T., & Martin, O. A. (2022). Bambi: A simple interface for fitting Bayesian linear models in python. *Journal of Statistical Software*, *103*(15), 1–29. https://doi.org/10.18637/jss.v103.i15

Chen, L., Aalto, J., & Luoto, M. (2021). Significant shallow-depth soil warming over Russia during the past 40 years. *Global and Planetary Change*, *197*, 103394. https://doi.org/10.1016/j.gloplacha.2020.103394

Chen, X., Jeong, S., Park, C.-E., Park, H., Joo, J., Chang, D., & Yun, J. (2022). Different responses of surface freeze and thaw phenology changes to warming among Arctic permafrost types. *Remote Sensing of Environment*, *272*, 112956. https://doi.org/10.1016/j.rse.2022.112956

Christiansen, H. H., Gilbert, G. L., Demidov, N., Guglielmin, M., Isaksen, K., Osuch, M., & Boike, J. (2020a). Permafrost temperatures and active layer thickness in Svalbard during 2017/2018 (PermaSval). Retrieved from https://sios-svalbard.org/SESS_Issue2

Christiansen, H. H., Gilbert, G. L., Neumann, U., Demidov, N., Guglielmin, M., Isaksen, K., et al. (2020b). Ground ice content, drilling methods and equipment and permafrost dynamics in Svalbard 2016–2019 (PermaSval). https://doi.org/10.5281/zenodo.4294095

Dahlke, S., Hughes, N. E., Wagner, P. M., Gerland, S., Wawrzyniak, T., Ivanov, B., & Maturilli, M. (2020). The observed recent surface air temperature development across Svalbard and concurring footprints in local sea ice cover. *International Journal of Climatology*, *40*(12), 5246–5265. https://doi.org/10.1002/joc.6517

Farquharson, L. M., Romanovsky, V. E., Cable, W. L., Walker, D. A., Kokelj, S., & Nicolsky, D. (2019). Climate change drives widespread and rapid thermokarst development in very cold permafrost in the Canadian High Arctic. *Geophysical Research Letters*, *46*(12), 6681–6689. https://doi.org/10.1029/2019GL082187

Førland, E. J., Isaksen, K., Lutz, J., Hanssen-Bauer, I., Vikhamar Schuler, T., Dobler, A., et al. (2020). Measured and modeled historical precipitation trends for Svalbard. *Journal of Hydrometeorology*, *21*(6), 1279–1296. https://doi.org/10.1175/JHM-D-19-0252.1

Gelman, A., Carlin, J. B., Stern, H. S., Dunson, D. B., Vehtari, A., & Rubin, D. B. (2013). *Bayesian data analysis* (3rd ed.). CRC Press. https://doi.org/10.1201/b16018

Gjelten, H. M., Nordli, Ø., Isaksen, K., Førland, E. J., Sviashchennikov, P. N., Wyszynski, P., et al. (2016). Air temperature variations and gradients along the coast and fjords of western Spitsbergen. *Polar Research*, *35*(1), 29878. https://doi.org/10.3402/polar.v35.29878

Groenke, B., Langer, M., Nitzbon, J., Westermann, S., Gallego, G., & Boike, J. (2023). Investigating the thermal state of permafrost with Bayesian inverse modeling of heat transfer. *The Cryosphere*, *17*(8), 3505–3533. https://doi.org/10.5194/tc-17-3505-2023

Groisman, P. Y., Bulygina, O. N., Yin, X., Vose, R. S., Gulev, S. K., Hanssen-Bauer, I., & Førland, E. (2016). Recent changes in the frequency of freezing precipitation in North America and northern Eurasia. *Environmental Research Letters*, *11*(4), 045007. https://doi.org/10.1088/1748-9326/11/4/045007

Grünberg, I., Miesner, F., Bornemann, N., Cable, W. L., & Boike, J. (2024a). Meteorological and soil data from Bayelva, Svalbard, homogenised data product (version 1: 1998-09-13 to 2023-12-31, design 2: One row per time-step) [Dataset]. *PANGAEA*. https://doi.pangaea.de/10.1594/PANGAEA.969342

Grünberg, I., Miesner, F., Bornemann, N., Cable, W. L., & Boike, J. (2024b). Meteorological and soil data from Bayelva, Svalbard, homogenised data product (1998 et seq.) [Dataset bundled publication]. *PANGAEA*. https://doi.pangaea.de/10.1594/PANGAEA.969343

Hansen, B. B., Isaksen, K., Benestad, R. E., Kohler, J., Pedersen, Å. Ø., Loe, L. E., et al. (2014). Warmer and wetter winters: Characteristics and implications of an extreme weather event in the high Arctic. *Environmental Research Letters*, *9*(11), 114021. https://doi.org/10.1088/1748-9326/9/11/114021

Hanssen-Bauer, I., Førland, E., Hisdal, H., Mayer, S., Sandø, A., & Sorteberg, A. (Eds.) (2019). *Climate in Svalbard 2100 – A knowledge base for climate adaptation*. (NCCS report 1/2019). https://doi.org/10.25607/OBP-888

Hoffman, M. D., & Gelman, A. (2014). The No-U-Turn sampler: Adaptively setting path lengths in Hamiltonian Monte Carlo. *Journal of Machine Learning Research*, *15*(47), 1593–1623. Retrieved from http://jmlr.org/papers/v15/hoffman14a.html

Isaksen, K., Lutz, J., Sorensen, A. M., Godoy, O., Ferrighi, L., Eastwood, S., & Aaboe, S. (2022a). Advances in operational permafrost monitoring on Svalbard and in Norway. *Environmental Research Letters*, *17*(9), 095012. https://doi.org/10.1088/1748-9326/ac8e1c

Isaksen, K., Nordli, Ø., Førland, E. J., Łupikasza, E., Eastwood, S., & Niedźwiedź, T. (2016). Recent warming on Spitsbergen – Influence of atmospheric circulation and sea ice cover. *Journal of Geophysical Research: Atmospheres*, *121*(20), 11913–11931. https://doi.org/10.1002/2016JD025606

Isaksen, K., Nordli, Ø., Ivanov, B., Køltzow, M. A. Ø., Aaboe, S., Gjelten, H. M., et al. (2022b). Exceptional warming over the Barents area. *Scientific Reports*, *12*(1), 9371. https://doi.org/10.1038/s41598-022-13568-5

Isaksen, K., Sollid, J. L., Holmlund, P., & Harris, C. (2007). Recent warming of mountain permafrost in Svalbard and Scandinavia. *Journal of Geophysical Research*, *112*(F2), F02S04. https://doi.org/10.1029/2006JF000522

Kim, Y., Kimball, J. S., Glassy, J., & Du, J. (2017). An extended global earth system data record on daily landscape freeze–thaw status determined from satellite passive microwave remote sensing. *Earth System Science Data*, *9*(1), 133–147. https://doi.org/10.5194/essd-9-133-2017

Lam, H. M., Geldsetzer, T., Howell, S. E. L., & Yackel, J. (2023). Snow depth on sea ice and on land in the Canadian Arctic from long-term observations. *Atmosphere-Ocean*, *61*(4), 217–233. https://doi.org/10.1080/07055900.2022.2060178

Lange, K. L., Little, R. J., & Taylor, J. M. (1989). Robust statistical modeling using the t distribution. *Journal of the American Statistical Association*, *84*(408), 881–896. https://doi.org/10.2307/2290063

Li, J., Wu, C., Peñuelas, J., Ran, Y., & Zhang, Y. (2023). The start of frozen dates over northern permafrost regions with the changing climate. *Global Change Biology*, *29*(16), 4556–4568. https://doi.org/10.1111/gcb.16752

Lilhare, R., Déry, S. J., Stadnyk, T. A., Pokorny, S., & Koenig, K. A. (2022). Warming soil temperature and increasing baseflow in response to recent and potential future climate change across northern Manitoba, Canada. *Hydrological Processes*, *36*(11), e14748. https://doi.org/10.1002/hyp.14748

Maturilli, M., Hanssen-Bauer, I., Neuber, R., Rex, M., & Edvardsen, K. (2019). The atmosphere above Ny-Ålesund: Climate and global warming, ozone and surface UV radiation. In H. Hop & C. Wiencke (Eds.), *The ecosystem of Kongsfjorden, Svalbard* (Vol. 2, pp. 23–46). Springer International Publishing. https://doi.org/10.1007/978-3-319-46425-1

Maturilli, M., Herber, A., & König-Langlo, G. (2015). Surface radiation climatology for Ny-Ålesund, Svalbard (78.9°N), basic observations for trend detection. *Theoretical and Applied Climatology*, *120*(1), 331–339. https://doi.org/10.1007/s00704-014-1173-4

McCrystall, M. R., Stroeve, J., Serreze, M., Forbes, B. C., & Screen, J. A. (2021). New climate models reveal faster and larger increases in Arctic precipitation than previously projected. *Nature Communications*, *12*(1), 6765. ISSN: 2041-1723. https://doi.org/10.1038/s41467-021-27031-y

Mohammadzadeh Khani, H., Kinnard, C., & Lévesque, E. (2022). Historical trends and projections of snow cover over the high Arctic: A review. *Water*, *14*(4), 587. https://doi.org/10.3390/w14040587

Mudryk, L. R., Derksen, C., Howell, S., Laliberté, F., Thackeray, C., Sospedra-Alfonso, R., et al. (2018). Canadian snow and sea ice: Historical trends and projections. *The Cryosphere*, *12*(4), 1157–1176. https://doi.org/10.5194/tc-12-1157-2018

Nicolsky, D. J., & Romanovsky, V. E. (2018). Modeling long-term permafrost degradation. *Journal of Geophysical Research: Earth Surface*, *123*(8), 1756–1771. https://doi.org/10.1029/2018JF004655

Nordli, Ø., Wyszynski, P., Gjelten, H. M., Isaksen, K., Lupikasza, E., Niedzwiedz, T., & Przybylak, R. (2020). Revisiting the extended Svalbard Airport monthly temperature series, and the compiled corresponding daily series 1898–2018. *Polar Research*, *39*(0), 1–15. https://doi.org/10.33265/polar.v39.3614

Orvin, A. K. (1944). Litt om kilder på Svalbard. *Norsk Geografisk Tidsskrift - Norwegian Journal of Geography*, *10*(1), 16–38. (In Norwegian). https://doi.org/10.1080/00291954408621804

Osuch, M., & Wawrzyniak, T. (2017). Variations and changes in snow depth at meteorological stations Barentsburg and Hornsund (Spitsbergen). *Annals of Glaciology*, *58*(75pt1), 11–20. https://doi.org/10.1017/aog.2017.20

Peeters, B., Pedersen, Å. Ø., Loe, L. E., Isaksen, K., Veiberg, V., Stien, A., et al. (2019). Spatiotemporal patterns of rain-on-snow and basal ice in high Arctic Svalbard: Detection of a climate-cryosphere regime shift. *Environmental Research Letters*, *14*(1), 015002. https://doi.org/10.1088/1748-9326/aaefb3

Pomeroy, J. W., & Brun, E. (2001). Physical properties of snow. In *Snow ecology: An interdisciplinary examination of snow-covered ecosystems*.

Rantanen, M., Karpechko, A. Y., Lipponen, A., Nordling, K., Hyvärinen, O., Ruosteenoja, K., et al. (2022). The Arctic has warmed nearly four times faster than the globe since 1979. *Communications Earth & Environment*, *3*(1), 168. https://doi.org/10.1038/s43247-022-00498-3

Rinke, A., Maturilli, M., Graham, R. M., Matthes, H., Handorf, D., Cohen, L., et al. (2017). Extreme cyclone events in the Arctic: Wintertime variability and trends. *Environmental Research Letters*, *12*(9), 094006. https://doi.org/10.1088/1748-9326/aa7def

Riseborough, D. W. (1990). Soil latent heat as a filter of the climate signal in permafrost. In *Proceedings of the 5th Canadian Permafrost Conference* (Vol. 54, pp. 199–205). Université Laval. Retrieved from https://pubs.aina.ucalgary.ca/cpc/CPC5-199.pdf

Schuh, C., Frampton, A., & Christiansen, H. H. (2017). Soil moisture redistribution and its effect on inter-annual active layer temperature and thickness variations in a dry loess terrace in Adventdalen, Svalbard. *The Cryosphere*, *11*(1), 635–651. https://doi.org/10.5194/tc-11-635-2017

Smith, S. L., O'Neill, H. B., Isaksen, K., Noetzli, J., & Romanovsky, V. E. (2022). The changing thermal state of permafrost. *Nature Reviews Earth & Environment*, *3*(1), 10–23. https://doi.org/10.1038/s43017-021-00240-1

Sobota, I., Weckwerth, P., & Grajewski, T. (2020). Rain-On-Snow (ROS) events and their relations to snowpack and ice layer changes on small glaciers in Svalbard, the high Arctic. *Journal of Hydrology*, *590*, 125279. https://doi.org/10.1016/j.jhydrol.2020.125279

Strand, S. M., Christiansen, H. H., & Gilbert, G. L. (2022). Permafrost thermal dynamics and cryostratigraphy at Villum Research Station, Station Nord, Eastern North Greenland (81 degrees N). *Journal of Geophysical Research: Earth Surface*, *127*(4), e2021JF006502. https://doi.org/10.1029/2021JF006502

Strand, S. M., Christiansen, H. H., Johansson, M., Åkerman, J., & Humlum, O. (2021). Active layer thickening and controls on interannual variability in the Nordic Arctic compared to the circum-Arctic. *Permafrost and Periglacial Processes*, *32*(1), 47–58. https://doi.org/10.1002/ppp.2088

Streletskiy, D. A., Sherstiukov, A. B., Frauenfeld, O. W., & Nelson, F. E. (2015). Changes in the 1963–2013 shallow ground thermal regime in Russian permafrost regions. *Environmental Research Letters*, *10*(12), 125005. https://doi.org/10.1088/1748-9326/10/12/125005

The Norwegian Meteorological Institute (MET Norway). (2024). Seklima – Observations and weather statistics. Retrieved from https://seklima.met.no/

van Pelt, W. J. J., Kohler, J., Liston, G. E., Hagen, J. O., Luks, B., Reijmer, C. H., & Pohjola, V. A. (2016). Multidecadal climate and seasonal snow conditions in Svalbard. *Journal of Geophysical Research: Earth Surface*, *121*(11), 2100–2117. https://doi.org/10.1002/2016JF003999

van Pelt, W. J. J., Pohjola, V., Pettersson, R., Marchenko, S., Kohler, J., Luks, B., et al. (2019). A long-term dataset of climatic mass balance, snow conditions, and runoff in Svalbard (1957–2018). *The Cryosphere*, *13*(9), 2259–2280. https://doi.org/10.5194/tc-13-2259-2019

Vasiliev, A. A., Drozdov, D. S., Gravis, A. G., Malkova, G. V., Nyland, K. E., & Streletskiy, D. A. (2020). Permafrost degradation in the Western Russian Arctic. *Environmental Research Letters*, *15*(4), 045001. https://doi.org/10.1088/1748-9326/ab6f12

Vickers, H., Karlsen, S. R., & Malnes, E. (2020). A 20-year MODIS-based snow cover dataset for Svalbard and its link to phenological timing and sea ice variability. *Remote Sensing*, *12*(7), 1123. https://doi.org/10.3390/rs12071123

Vickers, H., Malnes, E., & Eckerstorfer, M. (2022). A synthetic aperture radar based method for long term monitoring of seasonal snowmelt and wintertime rain-on-snow events in Svalbard. *Frontiers in Earth Science*, *10*, 868945. https://doi.org/10.3389/feart.2022.868945

Vihma, T. (2014). Effects of Arctic sea ice decline on weather and climate: A review. *Surveys in Geophysics*, *35*(5), 1175–1214. https://doi.org/10.1007/s10712-014-9284-0

Vihma, T., Screen, J., Tjernström, M., Newton, B., Zhang, X., Popova, V., et al. (2016). The atmospheric role in the Arctic water cycle: A review on processes, past and future changes, and their impacts. *Journal of Geophysical Research: Biogeosciences*, *121*(3), 586–620. https://doi.org/10.1002/2015JG003132

Walker, D. A., Raynolds, M. K., Daniëls, F. J. A., Einarsson, E., Elvebakk, A., Gould, W. A., et al. (2005). The Circumpolar Arctic vegetation map. *Journal of Vegetation Science*, *16*(3), 267–282. https://doi.org/10.1111/j.1654-1103.2005.tb02365.x

Walvoord, M. A., & Kurylyk, B. L. (2016). Hydrologic impacts of thawing permafrost – A review. *Vadose Zone Journal*, *15*(6), 1–20. https://doi.org/10.2136/vzj2016.01.0010

Wang, K., Jafarov, E., Schaefer, K., Overeem, I., Romanovsky, V., Clow, G., et al. (2018). A synthesis dataset of permafrost-affected soil thermal conditions for Alaska, USA. *Earth System Science Data Discussions*, *10*, 1–22. https://doi.org/10.5194/essd-2018-54

Westermann, S., Boike, J., Langer, M., Schuler, T. V., & Etzelmüller, B. (2011). Modeling the impact of wintertime rain events on the thermal regime of permafrost. *The Cryosphere*, *5*(4), 945–959. https://doi.org/10.5194/tc-5-945-2011

Westermann, S., Lüers, J., Langer, M., Piel, K., & Boike, J. (2009). The annual surface energy budget of a high-Arctic permafrost site on Svalbard, Norway. *The Cryosphere*, *3*(2), 245–263. https://doi.org/10.5194/tc-3-245-2009

Wickström, S., Jonassen, M. O., Cassano, J. J., & Vihma, T. (2020). Present temperature, precipitation, and rain-on-snow climate in Svalbard. *Journal of Geophysical Research: Atmospheres*, *125*(14), e2019JD032155. https://doi.org/10.1029/2019JD032155

Wiecki, T., Salvatier, J., Vieira, R., Kochurov, M., Patil, A., Willard, B. T., et al. (2023). Pymc-devs/pymc: V5.0.2. *Zenodo*. https://doi.org/10.5281/zenodo.7552029